Thin-Walled Structures 98 (2016) 312–331

Contents lists available at ScienceDirect

Thin-Walled Structures

journal homepage: www.elsevier.com/locate/tws

Performance of cold-formed-steel-framed shear walls sprayed with lightweight mortar under reversed cyclic loading

Bin Liu [a,*], Ji-Ping Hao [a], Wei-Hui Zhong [a], Hao Wang [b]

[a] Department of Civil Engineering, Xi'an University of Architecture and Technology, Xi'an, PR China
[b] CRUPE Framing (UK) Ltd., Twickenham, Greater London, UK

ARTICLE INFO

Article history:
Received 17 July 2014
Received in revised form
20 April 2015
Accepted 24 September 2015

Keywords:
Cold-formed steel
Shear wall
Sprayed lightweight mortar
Calcium silicate board
Reversed cyclic loading

ABSTRACT

Sheathing with sprayed lightweight mortar (SLM) is proposed to enhance the performance of shear walls framed with cold-formed steel (CFS). Full-scale specimens were tested to assess the failure mode, strength, stiffness, ductility, and energy absorption achieved. Slippage between the CFS framing and the SLM significantly increased the walls' strength and stiffness and restricted crack propagation. The failure mode typically involves local buckling of the end studs. Specimens with SLM on the front and calcium silicate boards (CSBs) on the back were weaker than specimens with SLM sheathing on both sides. Joint-strengthened knee elements or X-shaped steel-strap bracings increased the load-bearing capacity and reduced the ductility of the specimens.

1. Introduction

As alternatives to timber structures, structures framed with cold-formed steel (CFS), consisting of CFS members and lightweight sheathing, are suitable for load-bearing and enclosure systems in low-rise residential and commercial buildings. Because of their many advantages, which include light weight, dimensional stability, cost effectiveness, full recyclability, and workability, such structures have been widely employed in recent years in North America, Europe, Australia, Japan, and China. CFS-framed shear walls constitute the main force-resisting members of such structural systems, which typically consist of steel frames (including studs, tracks, blocking members, and bracing members) and lightweight sheathing attached to the CFS members by self-drilling screw connections. The shear walls support the vertical loads transferred from the floors and roofs, as well as horizontal wind and seismic loads. The mechanical behaviour of such structures under horizontal loads is complex. The relevant standard of the American Iron and Steel Institute, AISI S213 [1], was based on the results of a series of monotonic and cyclic tests conducted on CFS-framed shear walls by Serrette et al. [2–4].

Fülöp and Dubina [5] also conducted a series of monotonic and cyclic loading tests on full-scale CFS-framed walls with different types of sheathing, including walls made of corrugated sheets, gypsum boards, and oriented strand boards (OSBs). The results showed that the shear resistance of the wall panels was significant in terms of both rigidity and load-bearing capacity and that the hysteretic behaviour was characterised by significant pinching. Failure was initiated in the bottom track around the anchor bolt, and this heightened the need for strengthening the corners. The damage gradually increased in the seam fasteners until overall failure of the wall panels occurred.

Pan and Shan [6] conducted an experimental study on the structural strength of CFS-framed shear walls sheathed with gypsum boards, calcium silicate boards (CSBs), and OSB panels. Two aspect ratios, 1.0 and 2.0, were used in the design of the test specimens. The CFS walls with the OSB panels were found to have the highest ultimate strength, followed by the CFS walls with CSB panels and the CFS walls with gypsum boards. For the same aspect ratio, the ultimate strengths of the wall specimens with one-sided sheathing were approximately 50% of those of the specimens with two-sided sheathing. Design ductility ratios of 6.6, 3.8, and 3.9 were suggested for CFS-framed walls sheathed with gypsum boards, CSB panels, and OSB panels, respectively.

Nithyadharan [7] tested eight different CFS-framed shear walls sheathed with CSB panels and observed that the failure process involved titling, bearing, and pull-through of the screws, followed by complete separation and rigid body rotation of the CSB panels. The ultimate strength and energy dissipation increased with

* Correspondence to: Department of Civil Engineering, Xi'an University of Architecture and Technology, No. 13, Yanta Road, Xi'an 710055, Shaanxi Province, PR China.
E-mail address: liubin881113@gmail.com (B. Liu).

http://dx.doi.org/10.1016/j.tws.2015.09.024
0263-8231/

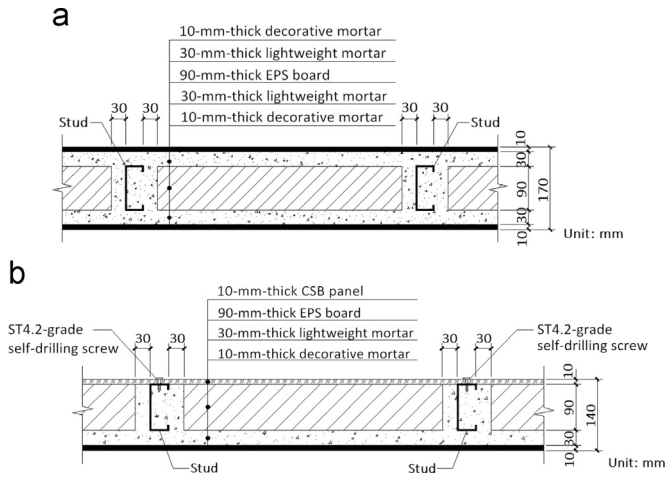

Fig. 1. Details of wall specimens: (a) wall specimen with SLM on both sides and (b) wall specimen with SLM on the front side and CSB panels on the back side.

increasing board thickness and screw edge distance. The wall panels with a Type B board arrangement (two boards with a discontinuity at the intermediate stud) underwent considerably larger deformations than those with a Type A board arrangement (a single board across which shear was transferred) because of the additional relative slippage at the screws in the interior studs of the former.

Liu [8] conducted a series of cyclic tests on full-scale CFS walls sheathed with OSB panels. The results indicated that the primary energy dissipation mechanism occurs at the fastener-to-sheathing connections and involves tilting, bearing, and pull-through. The use of interior gypsum boards was observed to increase the initial stiffness and modestly increase the strength, while the other behaviours were similar to those observed in cases with a ledger track and no interior gypsum board. Overall, the hysteretic behaviour of the CFS wall panels was found to include a severe pinching response. Equivalent energy elastic plastic (EEEP) and Pinching4 models fitted to the tested data were recommended for use in nonlinear history analysis.

Zeynalian [9] studied the structural behaviour of CFS-framed shear walls sheathed with fibre-cement boards (FCBs) under cyclic lateral loading and concluded that the lateral resistance of CFS walls sheathed with FCB panels under cyclic loading was satisfactory with regard to both the shear strength and ductility and that the design was thus usable in seismic regions. The removal of FCB panels from one side was observed to decrease both the strength and ductility of the wall, although this modification could be made efficiently when diagonal stud elements were used at the corners of the wall.

The US Army Corps of Engineers (USACOE) published TI 809-07 [10], which stipulates more stringent guidelines for the design of CFS-framed shear walls than the AISI Standard [1]. The USACOE standard suggests that in calculating the shear capacity of a CFS wall, it is reasonable to ignore the contribution of the sheathing on both sides and rely on only the strength of the CFS frame. Zeynalian [11–13] conducted experimental and numerical studies of CFS frames with knee elements and concluded that although CFS frames exhibit relatively high maximum drifts, their strengths are lower than those of X-shaped bracing systems. Knee-stud bracing systems can thus only be used in low-seismic-activity regions where the required lateral resistance capacity is low.

Moghimi [14,15] investigated the shear behaviour of CFS frames with steel-strap X-shaped bracing. The results showed that local and distortional buckling of the frame members occurred in stable modes and that strap-braced CFS frames could be used to provide a considerable amount of shear capacity after the appearance of the first signs of buckling. The addition of brackets to the four corners of a CFS frame could also be used to considerably improve the lateral performance of the frame assemblies. By choosing appropriate perforated straps, the strap alongside the distributed holes could be made to reach yielding, thus avoiding the tearing of the strap at the tension unit location or at the strap-to-frame connection.

Iuorio and Macillo [16,17] conducted experimental and theoretical studies to evaluate the seismic behaviour of CFS-strap-braced stud walls. Their results showed satisfactory agreement between the theoretically predicted and experimentally determined behaviour of the walls and connection systems in terms of shear capacity. The study results also highlighted the need for careful design of the wall corners because their behaviour might significantly affect the overall wall response. Moreover, the behaviour factor values provided by AISI S213 [1] were widely confirmed by the experimental tests, with the code values corresponding to the lower limits of the experimental results.

In recent years, some researchers have proposed new connecting and sheathing techniques to improve the shear resistance of CFS-framed shear walls. Serrette [18,19] used steel pins and structural adhesive to attach structural wood sheathing, and the

Table 1
Description of test specimens.

Number	Group	Specimen label[a]	Type of CFS frame	Type of sheathing	Wall thickness (mm)	Vertical loading (kN)
1	Type A	F-KB	Knee elements	No sheathing	90	30
2		F-XB	X-shaped bracing on both sides			
3	Type B	W-NB-1	No bracing	SLM on both sides	170	30
4		W-NB-2				60
5		W-KB-1	Knee elements			30
6		W-KB-2				60
7		W-KB-S-1	Knee elements with joint-strengthening			30
8		W-KB-S-2				60
9		W-XB-1	X-shaped bracing on both sides			30
10		W-XB-2				60
11	Type C	W-NB-CSB	No bracing	SLM on the front side and CSB panels on the back side	140	30
12		W-XB-CSB	X-shaped bracing on one side			

[a] The notations of the letters in the specimen labels are as follows: F: frame, W: wall, NB: no bracing, KB: knee-element bracing, XB: X-shaped bracing, CSB: calcium silicate board, S: joint-strengthening.

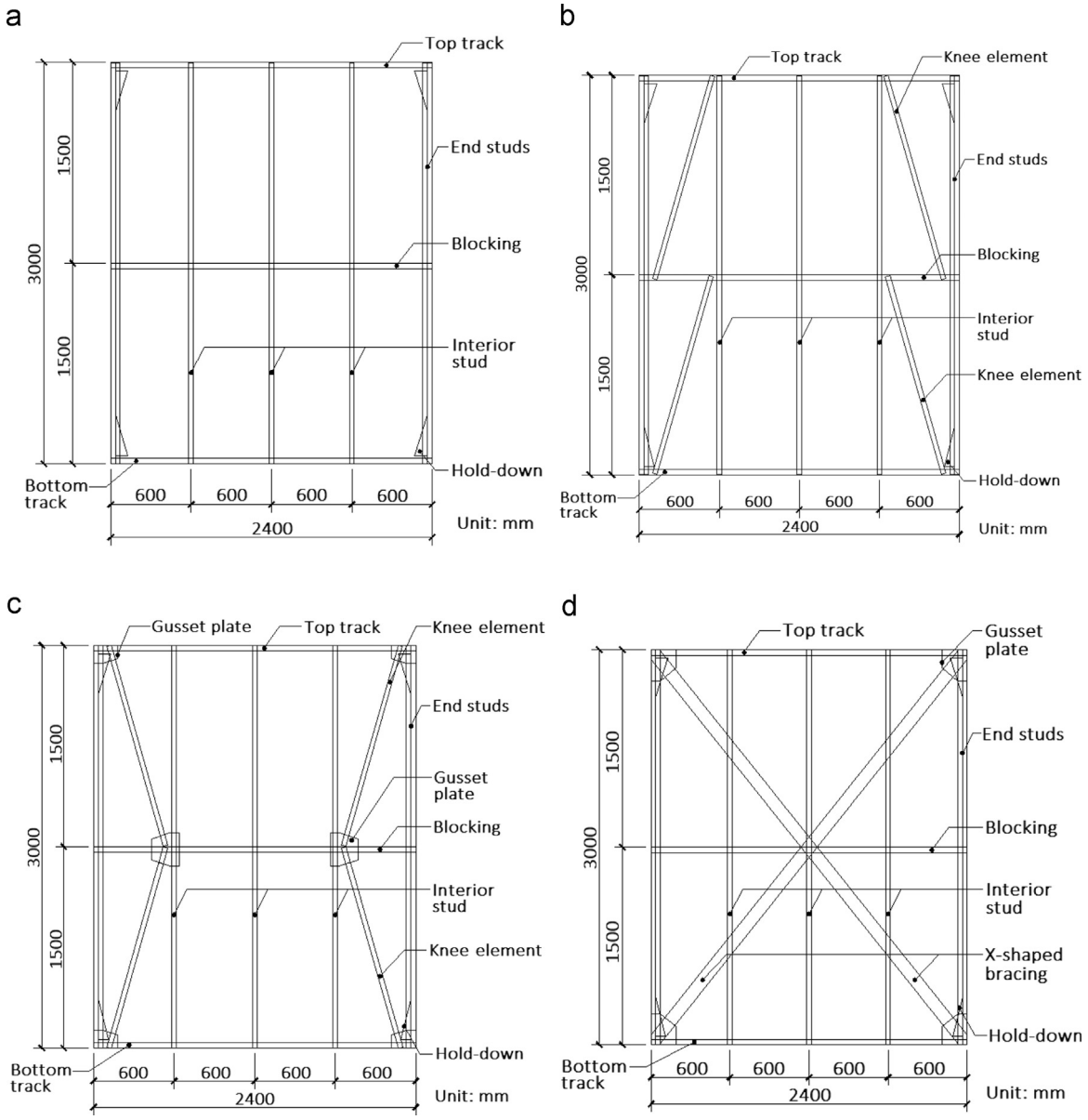

Fig. 2. Configurations of CFS frames: (a) CFS frame without bracing, (b) CFS frame with knee elements, (c) CFS frame with joint-strengthened knee elements, and (d) CFS frame with X-shaped bracings.

shear capacity was found to be roughly the same as that achieved using self-drilling screws. To decrease the required thickness of CFS-framed shear walls further, Yu [20,21], DaBreo [22], Shakibanasab [23], and Mohebbi [24] studied the shear behaviour of such walls with plain steel sheathing and found their strength and stiffness to be considerable. Vigh [25] used low-profile corrugated steel sheets instead of plain steel sheathing to reduce the out-of-plane deformation of the sheathing, and the corrugated shear wall was observed to exhibit higher shear strength and good ductility. Mowrtage [26] proposed a new sheathing technique whereby shotcreted ribbed steel sheets are used to improve the stability and load-bearing capacity of walls. He found that the lateral load-bearing capacity of walls sheathed using the proposed technique was approximately twice that of walls sheathed by traditional boards.

In engineering practice, complicated detailing of CFS-framed shear walls is needed to meet thermal, acoustic, and fire resistance requirements. In traditional construction, a thermal insulator in the form of expanded polystyrene (EPS) boards, extruded polystyrene (XPS) boards, or insulation cotton is placed inside the cavities or on the external surfaces of the steel frames. Breathable paper and waterproof membranes are also applied on the external facades of the walls to minimise energy loss by vapour exchange between the wall and the external environment.

To simplify the detailing of the walls, improve the thermal, acoustic, and fire resistance performance, and increase the stability and load-bearing capacity of the structure, a new sheathing technique for CFS-framed shear walls using sprayed lightweight mortar (SLM) is introduced in this paper. The construction procedure is as follows: (1) A thermal insulation material consisting of, for example, EPS boards or XPS boards, is placed in the cavity of the CFS frame, with a small gap left between the insulation material and the steel members. (2) Lightweight mortar is sprayed to fill the gap, ensuring that the CFS members are all covered. (3) Lightweight mortar of a certain thickness is sprayed on both sides of the CFS frame (Fig. 1a), or only on the front side of the wall, while the back side is sheathed with traditional boards (Fig. 1b). The SLM used in the shear walls is a type of gypsum

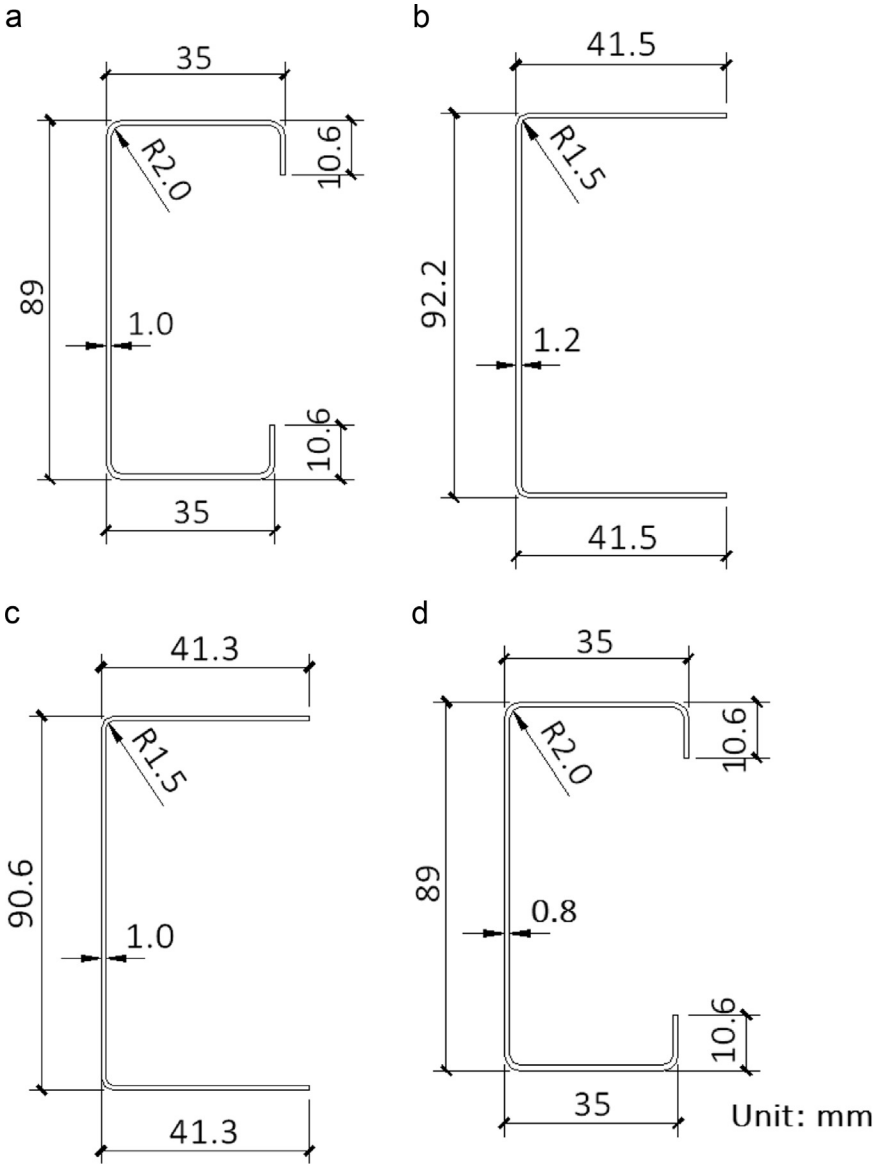

Fig. 3. Cross-sectional dimensions of CFS frame members: (a) stud, (b) track, (c) blocking, and (d) knee element.

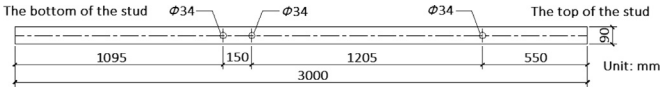

Fig. 4. Locations of pre-punched holes in studs.

mortar consisting mainly of the mortar mixture, polystyrene particles, and a mineral binder. After being sprayed, the material quickly hardens and develops substantial strength and ideal thermal, acoustic, and fire resistance properties. The material not only has a low carbon footprint but also significantly improves living standards.

To assess the shear behaviour of this new type of CFS-framed shear wall, two specimens of a CFS frame, eight specimens of a CFS-framed shear wall with SLM sheathing on both sides, and two specimens of a CFS-framed shear wall with SLM on the front side and CSB panels on the back side were tested under reversed cyclic loading. The hysteretic and envelope curves obtained are presented in this paper. The failure modes, load-bearing capacity, lateral stiffness, ductility, stiffness deterioration, and strain variation in the CFS members of the wall specimens were also analysed. The results of this study provide a basis for the theoretical analyses and engineering application of the proposed type of CFS wall.

2. Test programme

2.1. Test specimens

The test specimens were divided into three groups, namely, Type A, comprising CFS frames; Type B, comprising CFS-framed shear walls with SLM sheathing on both sides; and Type C, comprising CFS-framed shear walls with SLM sheathing on the front side and CSB panels on the back side. The details of the grouping, labelling, and description of the test specimens are presented in Table 1.

Each test specimen had an overall width of 2400 mm, a height of 3000 mm, and CFS studs spaced at 600 mm. In accordance with the Chinese Standard GB 50018-2002 [27], the specimens were fabricated using steel grade Q235B. The configurations of the steel frames are shown in Fig. 2. The CFS frame was composed of studs (89 mm web × 35 mm flange × 10.6 mm lip × 1.0 mm thickness), tracks (92.2 mm web × 41.5 mm flange × 1.2 mm thickness),

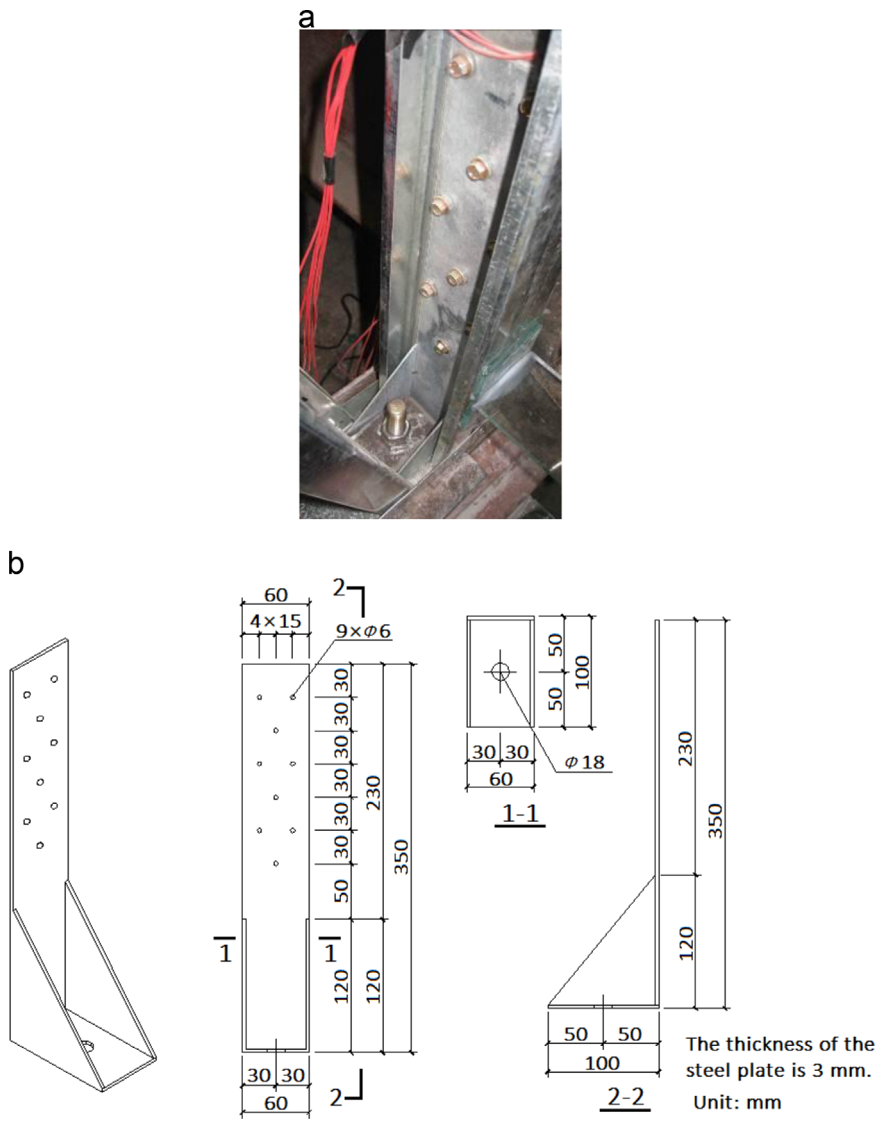

Fig. 5. Hold-down device: (a) connection with the test frame and (b) detailed dimensions of the hold-down device.

blocking members (90.6 mm web × 41.3 mm flange × 1.0 mm thickness), and diagonal bracing members, as shown in Fig. 3. The knee elements had the same sectional dimensions as the studs, except that their thickness was 0.8 mm. The steel-strap X-shaped bracing was 98 mm wide and 1.0 mm thick. In compliance with the Chinese Standard GB/T 15856-2002 [28], the CFS members were connected by ST4.8-grade (d=4.8 mm) wafer-head self-drilling screws. Two studs joined back to back by a single row of self-drilling screws spaced at 300 mm were used on the two vertical sides of the CFS frame. To facilitate the installation of service pipelines inside the wall frames, the web of each stud had three pre-punched circular holes 34 mm in diameter (Fig. 4), and another hole of the same diameter was punched in the centre of each knee element. The hold-down devices were attached to the web from the top or bottom of the end studs using nine 5.5-mm-diameter hex-head self-drilling screws and connected to the test frame by a 16-mm-diameter threaded-anchor rob, as shown in Fig. 5.

For the CFS frame with joint-strengthened knee elements (Fig. 2c), 1.8-mm-thick gusset plates were employed to connect the knee elements to the studs, tracks, and blockings using ST4.8-grade wafer-head self-drilling screws, as shown in Fig. 6a and b. This connection method was used to increase the stiffness of the connections and improve the utilisation rate of the knee elements. For the CFS frame with X-shaped bracings (Fig. 2d), 1.8-mm-thick gusset plates were also used to strengthen the connection with the aid of X-shaped bracings, as shown in Fig. 6c. The number of screws required was determined based on the principle that the strength of the groups of screws must be equal to the yield strength of the steel strap [29].

The construction procedure for the CFS-framed shear wall specimens with SLM sheathing on both sides (Type B) was as follows. First, the CFS frame was assembled (Fig. 7a). Second, 90-mm-thick EPS boards were placed in the cavity of the CFS frame, with a gap of 30 mm left between the EPS boards and the CFS members (Fig. 7b). Third, lightweight mortar was sprayed into the gap, ensuring that all the CFS members were completely covered by the mortar (Fig. 7c). Finally, 30-mm-thick lightweight mortar and 10-mm-thick decorative mortar were sprayed on both sides of the CFS frame (Fig. 7d). The details of the Type B wall specimens are shown in Fig. 1a. The details of the CFS-framed shear wall specimens with SLM sheathing on the front side and 10-mm-thick CSB panels on the back side (Type C) were essentially the same as those of the Type B wall specimens, with the exception that CSB panels instead of lightweight mortar were used to sheath the back side (Fig. 1b). The CSB panels were attached to one face of the CFS

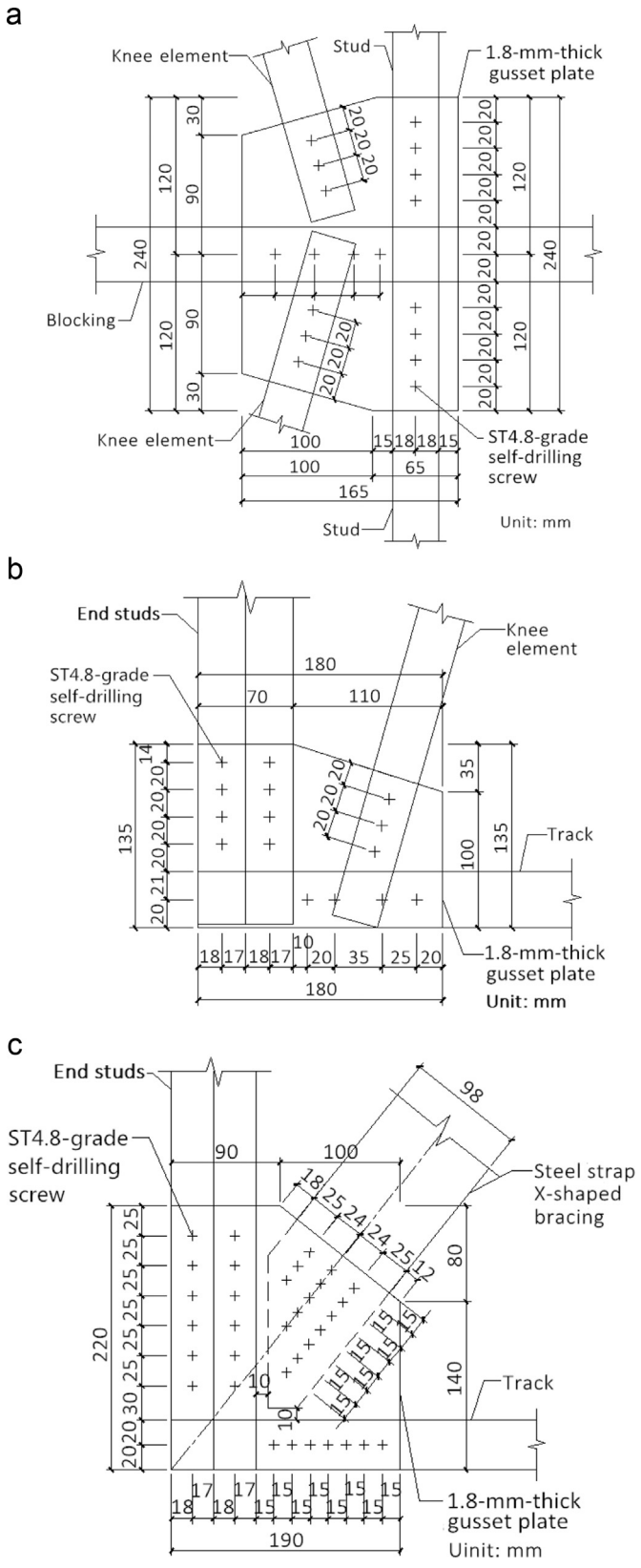

Fig. 6. Details of connections: (a) connection of knee elements to studs and blockings, (b) connection of knee elements to tracks and end studs, and (c) connection of X-shaped bracings to tracks and end studs.

frame using ST4.2-grade (d=4.2 mm) self-drilling bugle-head screws spaced at 150 mm at the periphery of the frame members and interior studs and blocking members spaced at 300 mm, as shown in Fig. 8. Because one piece of the CSB panel was 2440 mm × 1220 mm, three pieces had to be jointed in the horizontal direction. To facilitate observation of cracking of the wall during the test, a coat of white paint was applied to the wall surface.

2.2. Material properties

The material properties of the CFS members were tested in accordance with the Chinese Standard GB/T 228.1-2010 [30]. The results are summarised in Table 2. The compressive strength and elastic modulus of the lightweight mortar and decorative mortar used in the test were measured in accordance with the Chinese Standard JGJ/T 70-2009 [31]. The results are presented in Table 3. The 10-mm-thick CSB panels were orthotropic, and their density, elastic modulus, and flexural strength along their major and minor axes were determined in accordance with the Chinese Standard GB/T 17657-1999 [32]. The results are presented in Table 4.

2.3. Test setup

The experiments were performed in the Structures and Seismic Laboratory at Xi'an University of Architecture and Technology. The configuration of the test setup is shown in Fig. 9. Vertical loads were applied to the test specimens by a 200-kN hydraulic jack. A sliding guide was installed between the top reaction beam and the hydraulic jack to synchronise the loading point with the horizontal movement of the test specimens. Horizontal cyclic loads were applied by a 250-kN MTS actuator with a displacement range of ± 125 mm. Lateral bracing was installed on top of the wall specimens to prevent out-of-plane deformation of the specimens, thereby ensuring only in-plane deformation. The tracks of the wall specimens were connected to the top spreader beam and the bottom reaction beam by eight 16-mm-diameter high-strength friction-grip bolts to facilitate transfer of the horizontal shear load. Because the vertical loads applied to the wall specimens were resisted by the studs, as has also been observed in engineering practice, 20-mm-thick steel backing plates were placed on the top and bottom tracks, which correspond to the locations of the studs, to ensure a proper vertical load transfer path.

2.4. Loading protocols

The vertical loads listed in Table 1 were applied once and maintained during each test. For the horizontal cyclic loading protocol for Specimen F-KB, the displacement control method based on Method B of the ASTM Standard [33] was employed because of the relatively low shear capacity and lateral stiffness of the specimen. In accordance with Ref. [13], the loading protocol consisted of one full cycle at lateral amplitudes corresponding to 1.25%, 2.5%, 5%, 7.5%, and 10% of the ultimate displacement and three full cycles at amplitudes corresponding to 20%, 40%, 60%, 80%, 100%, 120%, 140%, 160%, and 180% of the ultimate displacement. In accordance with Appendix B of the Chinese Standard JGJ 227-2011 [34], the loading protocols for all the other wall specimens utilised the force–displacement combined control method. Before yielding of the wall specimens, a load increment of 3 kN was implemented in one full cycle. After yielding, the displacement control method was applied, wherein one increment of the yield displacement during three full cycles was implemented until the load decreased to 80% of the peak load. The yield displacements of the wall specimens were determined using the test results in Ref. [35].

Fig. 7. Construction procedure of wall specimens with SLM on both sides: (a) assembling of the CFS members, (b) installation of the EPS boards, (c) covering of the CFS members with mortar, and (d) spraying of lightweight mortar on both sides.

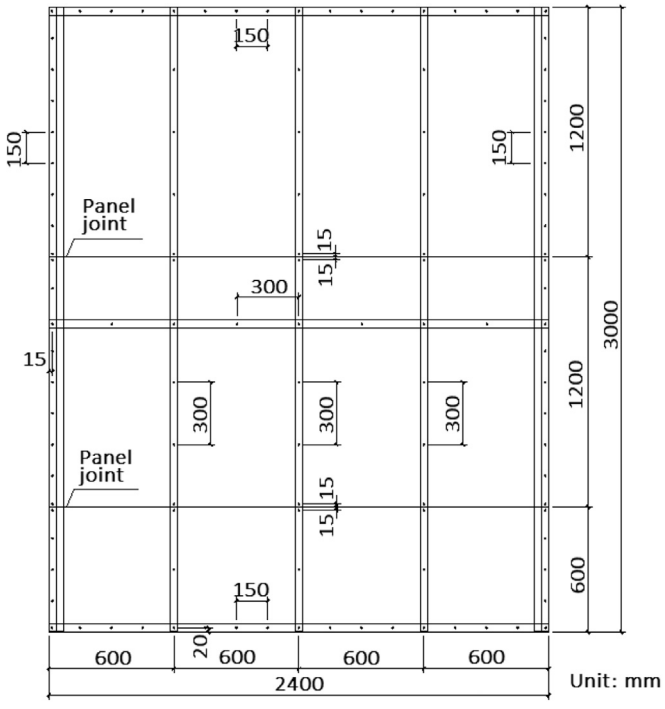

Fig. 8. Connection of CSB panels to CFS frame.

Table 2
Material properties of steel.

Nominal thickness (mm)	Yield stress (F_y) (MPa)	Ultimate stress (F_u) (MPa)	Elastic modulus (MPa)	Elongation (%)
0.8	288.80	336.90	1.99×10^5	26.25
1.0	290.08	351.82	1.94×10^5	29.81
1.2	291.32	352.51	1.95×10^5	34.21
1.8	303.50	361.71	1.91×10^5	37.73

Table 3
Material properties of lightweight mortar and decorative mortar.

Material type	Material name[a]	Compressive strength (MPa)	Elastic modulus (MPa)
Lightweight mortar	INSULTERM 600	1.67	1860
Decorative mortar	MYCA 63	13.62	12,760

[a] Material names according to Guangzhou CRUPE System Building Materials Co., Ltd.

2.5. Instrumentation

Eight linear variable differential transformers (LVDTs) were used in the tests, as shown in Fig. 10. One LVDT (D1) was used to

Table 4
Material properties of CSB panels.

Density (kg/m^3)	Elastic modulus (MPa)		Flexural strength (MPa)	
	Major axis	Minor axis	Major axis	Minor axis
1370	7450	5370	14.04	9.32

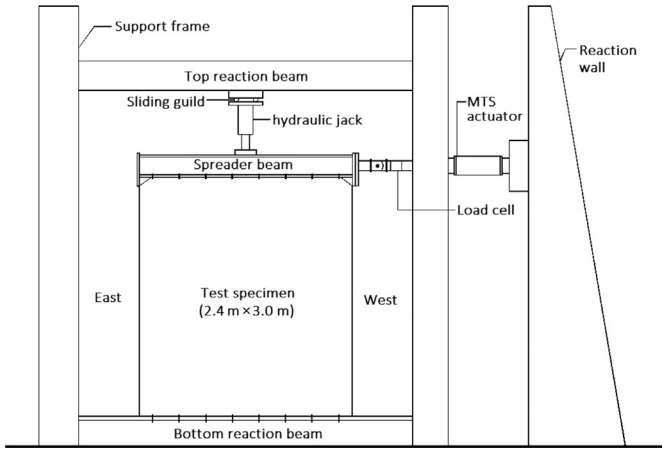

Fig. 9. Setup of test specimens.

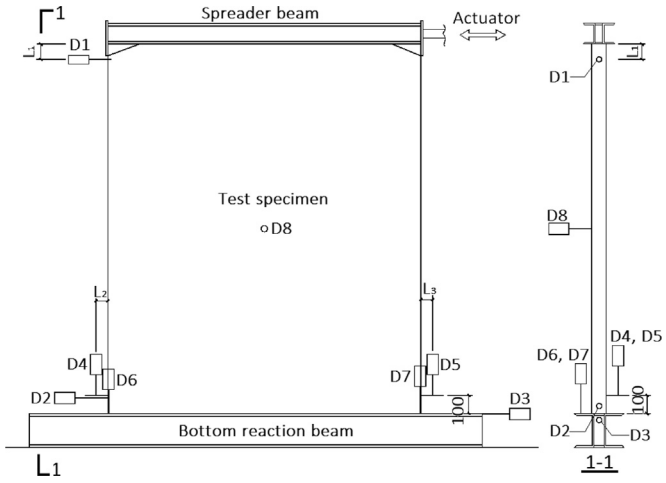

Fig. 10. Locations of LVDTs on test specimens.

measure the gross in-plane horizontal displacement. Two LVDTs (D2 and D3) were used to measure the relative slippage between the wall specimen and the bottom reaction beam. Four LVDTs (D4–D7) were used to measure the vertical displacements on the east and west sides at the bottom of the wall panel, relative to the bottom reaction beam. One LVDT (D8) was used to measure the out-of-plane deformation at the centre of the wall panel. To determine the strain variations in the CFS frame members, including the studs, tracks, blocking members, knee elements, and steel-strap X-shaped bracings, the strain gauges were arranged on the wall specimen as shown in Fig. 11. The strain gauges were placed on both sides of the X-shaped bracings at the same location to enable observation of the buckling of the steel strap. For the sections of the other steel member, the strain gauges were located at the centre of the flange. All the LVDTs and strain gauges were connected to a data logger for automatic data acquisition during the testing.

The in-plane displacement Δ_t measured by LVDT D1 consisted of three components, namely, the net in-plane displacement Δ_{net}

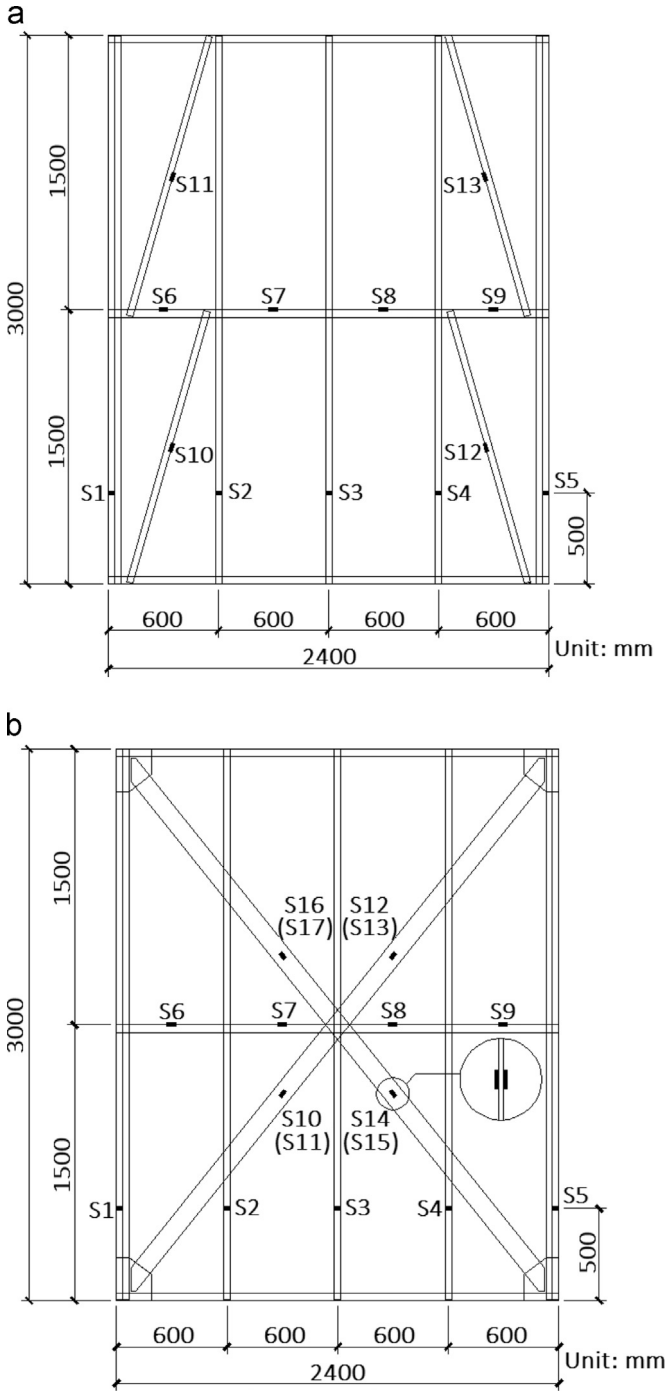

Fig. 11. Locations of strain gauges on test specimens: (a) CFS frame with knee elements and (b) CFS frame with X-shaped bracings.

due to the shear deformation of the wall specimens, the rigid body deformation Δ_s caused by the slippage between the wall specimen and the bottom reaction beam, and the deformation due to the rigid rotation of the wall specimen, as shown in Fig. 12. The net in-plane displacement Δ_{net}, which can be used to analyse the shear capacity of a wall specimen, is calculated as follows:

$$\Delta_{net} = \Delta_t - \Delta_s - \Delta_\varphi \quad (1)$$

$$\Delta_t = \frac{H}{H - L_1} \times \Delta_1 \quad (2)$$

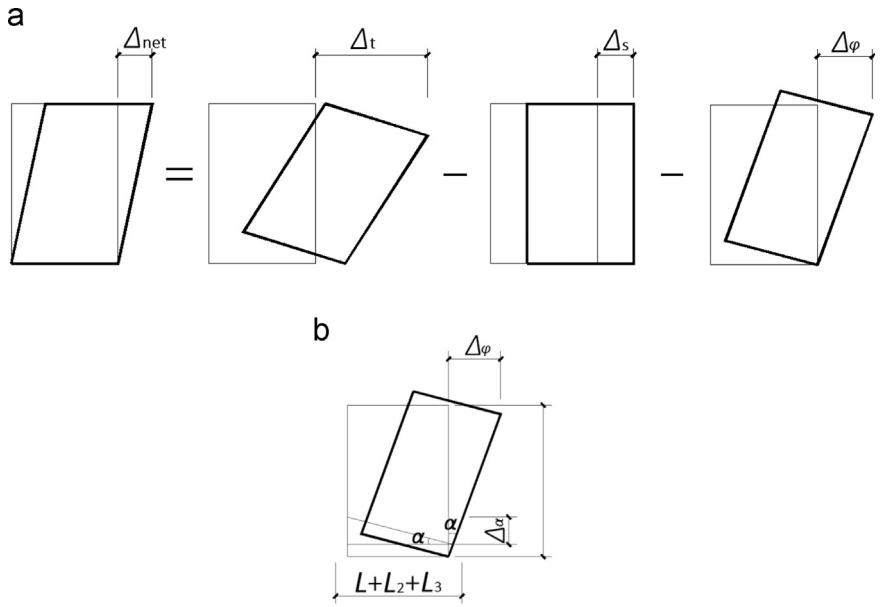

Fig. 12. Calculation of net in-plane deformation: (a) constitution of the horizontal deformation and (b) rigid rotation of the wall panel.

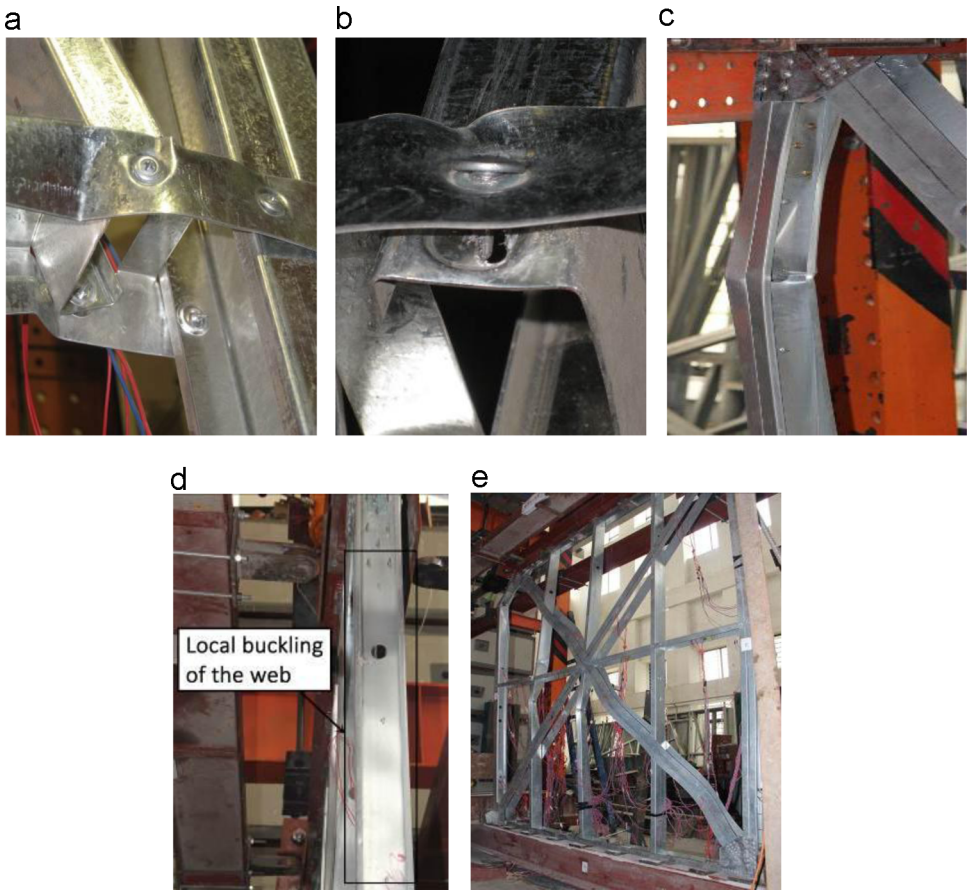

Fig. 13. Failure modes of CFS frame (Type A): (a) local buckling of the connection, (b) screw pull-out, (c) flexural–torsional buckling of the end studs, (d) local buckling of the web, and (e) flexural–torsional buckling of the interior studs.

$$\Delta_s = \Delta_2 - \Delta_3 \tag{3}$$

$$\Delta_\varphi = \frac{\Delta_\alpha}{L + L_2 + L_3} H = \frac{H}{L + L_2 + L_3} \times [(\Delta_5 - \Delta_7) - (\Delta_4 - \Delta_6)] \tag{4}$$

where the displacements $\Delta_1 - \Delta_7$ are measured by LVDTs D1–D7, as shown in Fig. 10; H is the height of the wall specimen; L is the width of the wall specimens; L_1 is the distance from LVDT D1 to the top of the wall; and L_2 and L_3 are the distances from the end of the wall panel to LVDTs D4 and D5, respectively.

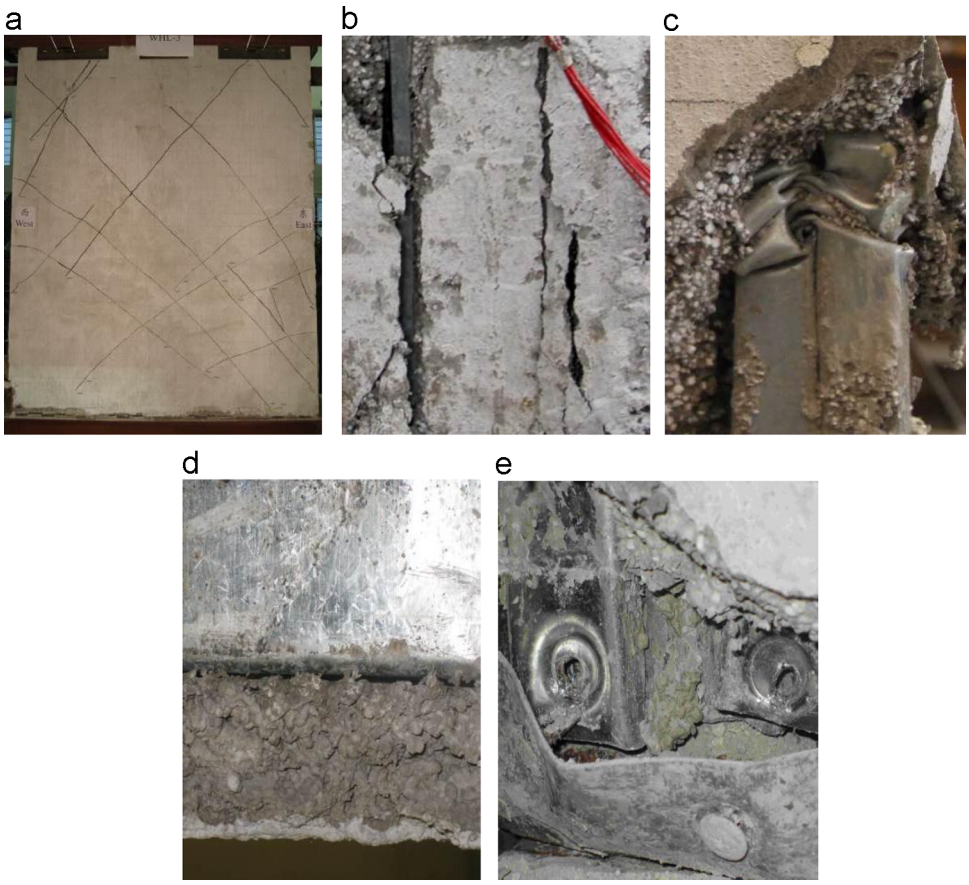

Fig. 14. Failure modes of wall specimens (Type B): (a) cracking of the mortar layer, (b) separation of the SLM layer from the bottom of the end studs, (c) local buckling of the bottom of the end studs, (d) slip between the CFS frame and the SLM layer, and (e) screw pull-out.

3. Failure phenomena

3.1. Type A specimens

In Specimen F-KB, continuous increase in the horizontal displacement caused the self-drilling screws used to attach the knee elements to the blockings to begin to tilt. At the peak load, the connections of the blockings to the knee elements experienced severe local buckling (Fig. 13a), resulting in the pull-out of the self-drilling screws (Fig. 13b).

In Specimen F-XB, because the width-to-thickness ratio of the steel strap was relatively large, the steel straps in the different directions could only bear the tensile forces under horizontal loading. During cyclic loading, there was alternating tightening of the tensile straps and slackening of the compressive straps, and only the tensile straps provided lateral resistance. At the stage of the 12-mm cycle, flexural–torsional buckling of the end studs on the west side occurred (Fig. 13c). As the horizontal displacement increased further, local buckling of the web occurred on the end studs (Fig. 13d), and flexural–torsional buckling of the interior studs occurred (Fig. 13e).

3.2. Type B specimens

When a Type B specimen was loaded to 27–36 kN, a diagonal crack first appeared in the mortar layer. As the load increased further, more crossing diagonal cracks appeared (Fig. 14a), and the SLM layer and the bottom of the end studs were gradually separated (Fig. 14b). When the peak load was reached, local buckling of the bottom of the end studs occurred (Fig. 14c). Meanwhile, relative slippage occurred between the CFS frame and the outside SLM layer (Fig. 14d). As the horizontal displacement increased further, the net section of the bottom of the end studs sometimes fractured under tension, and the self-drilling screws used to connect the end studs to the bottom track were pulled out (Fig. 14e). As the slippage between the steel frame and the outside SLM layer became more severe, the propagation of all the cracks was arrested.

3.3. Type C specimens

When the load applied to a Type C specimen was increased to 24–30 kN, cracks appeared in the mortar layer and at the corners of the CSB panels (Fig. 15a). As the load increased further, several crossing diagonal cracks appeared in the mortar layer (Fig. 15b). Relative movements of the individual CSB panels were observed, and the self-drilling screws along the edges of the panels failed by bearing or pull-through (Fig. 15c). At the peak load, local buckling of the bottom of the end studs occurred. As the horizontal displacement increased further, the CSB panels separated from the CFS frame due to the pull-through of the self-drilling screws along the edges of the panels (Fig. 15d).

4. Analysis of test results

4.1. Hysteresis curves

The hysteresis curves of the test specimens are shown in Fig. 16, where the abscissa represents the net in-plane displacement calculated using Eq. (1). The conclusions drawn from examination of the curves are as follows:

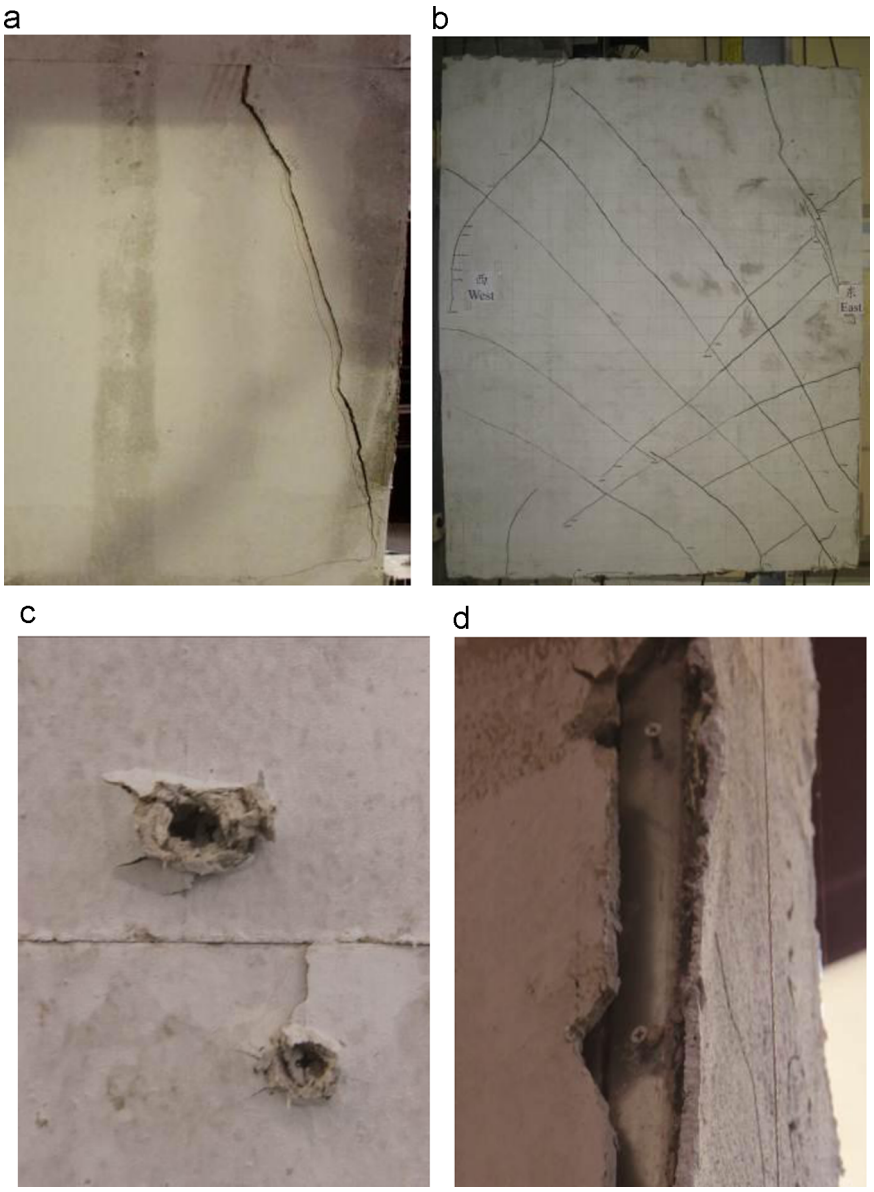

Fig. 15. Failure modes of wall specimens (Type C): (a) cracking of the corners of the CSB panels, (b) cracking of the mortar layer, (c) screw pull-though, and (d) separation of the CSB panels from the steel frame.

(1) In Specimen F-KB, because the studs cross through the webs of the blockings, the section of the blocking members at the joints is weakened. Together with the fact that the stiffness of the connections of the knee elements to the blocking members is weak, this causes both the load-bearing capacity and the lateral stiffness of the steel frame to be low. When failure occurs at a connection node of a knee element, there is an apparent degradation of the strength and stiffness of the steel frame. As the frame is completely unloaded, a certain degree of negative stiffness can be observed from the hysteresis curve.

(2) Owing to the relatively large width-to-thickness ratio of Specimen F-XB, the steel strap can only resist tension; it is hardly able to withstand compression. When completely unloaded, the tensile force acting on the steel strap is reduced to approximately zero, while the compressive strap provides no resistance to the lateral load. The 'no-load slip' phenomenon and the 'pinching' effect are therefore severe in the hysteresis curve.

(3) The Type B and Type C test specimens rapidly reach the elastic–plastic stage, and the hysteresis curves are spindle-shaped during the initial cycles. When unloaded, the specimens still exhibit residual deformation. As the load is increased, the hysteresis curve develops an arced shape, and a certain level of 'pinching' is observed. After the hysteresis curve changes from an arced shape to a reversed 'S' shape, the 'pinching' effect becomes distinct. At the same stage of the displacement amplitude cycle, the area of the hysteresis loops decreases with increasing loading cycles, and the load-bearing capacity and lateral stiffness also decrease. At the peak load, the hysteresis curve again gradually changes from a reversed 'S' shape to a 'Z' shape. This is caused by the failure of the self-drilling screws along the edges of the CSB panels, local buckling of the bottom of the end studs, and relative slippage between the steel frame and the SLM layer. The 'pinching' effect becomes progressively more severe, and apparent degradation of the strength and stiffness can be observed from the hysteresis curves.

(4) Appropriate increasing of in the vertical loads can be performed to improve the bonding–slippage behaviour between

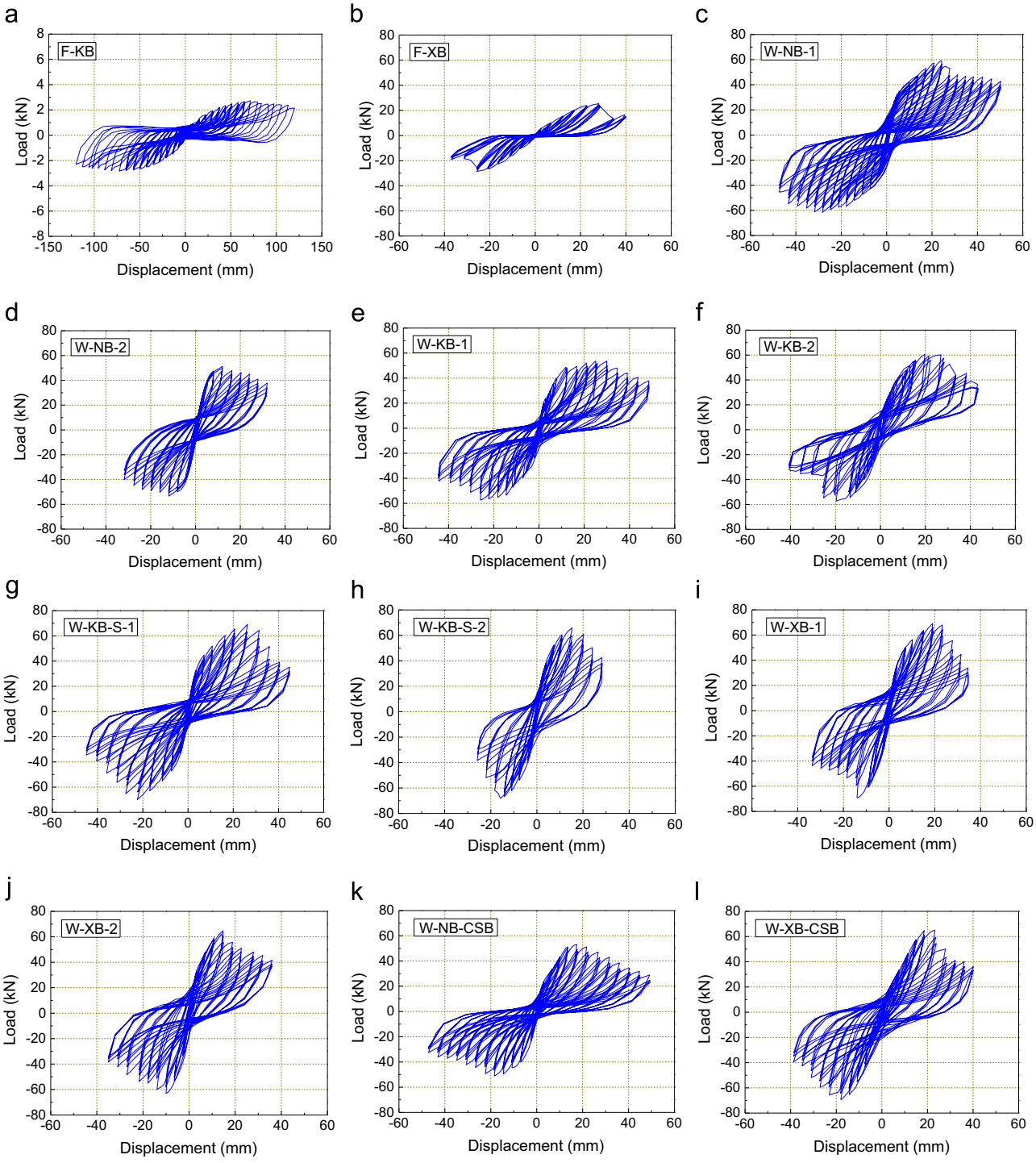

Fig. 16. Hysteresis curves of test specimens: (a) Specimen F-KB, (b) Specimen F-XB, (c) Specimen W-NB-1, (d) Specimen W-NB-2, (e) Specimen W-KB-1, (f) Specimen W-KB-2, (g) Specimen W-KB-S-1, (h) Specimen W-KB-S-2, (i) Specimen W-XB-1, (j) Specimen W-XB-2, (k) Specimen W-NB-CSB, and (l) Specimen W-XB-CSB.

the steel frame and the outside SLM layer. Hence, for a test specimen with the same specifications, increasing the vertical load will weaken the 'pinching' effect observed in the hysteresis curve, but the shear capacity will also be decreased.

(5) The installation of joint-strengthened knee elements and X-shaped bracings increases the load-bearing capacity of a wall with an SLM layer and also moderates the 'pinching' effect observed in the hysteresis curves.

4.2. Envelope curves

The envelope curves of the test specimens were obtained by enveloping the peak points of the force during the first cycle of cycles with the same displacement amplitude, as shown in Fig. 17. The following can be observed: (1) The envelope curves have no distinct yield point when the linear elastic stage is relatively short and the apparent non-linearity occurs at an early stage. (2) Because of the complete covering of the inner SLM and the strong interaction between the CFS frame and the outside SLM layer or CSB panels, the sheathed CFS walls have higher shear capacities

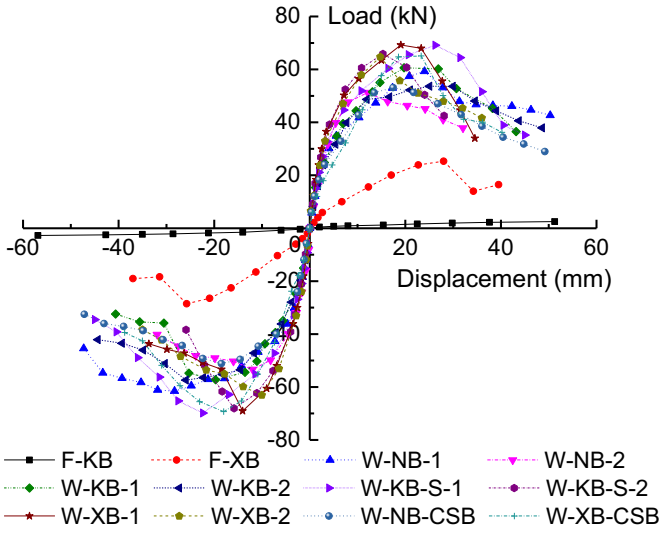

Fig. 17. The envelope curves of test specimens under cyclic loads.

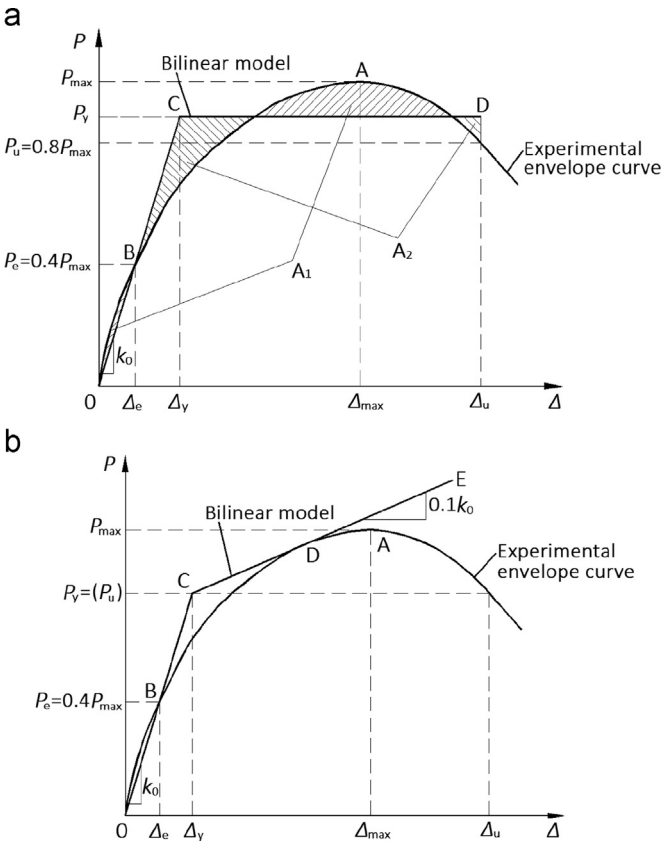

Fig. 18. Equivalent elastic–plastic bilinear model: (a) AISI Standard and (b) ECCS Recommendation.

and lateral stiffnesses than the simple CFS frames. (3) For wall specimens with the same specifications, increasing the vertical load decreases the load-bearing capacity and the corresponding lateral displacement at the peak force. However, the magnitude of the vertical load has little effect on the trend of the envelope curves at the early stage of the loading.

4.3. Characteristic values of loads and displacements

The characteristic values of the loads and displacements, including the elastic load P_e, yield load P_y, peak load P_{max}, and ultimate load P_u, as well as the corresponding lateral displacements Δ_e, Δ_y, Δ_{max}, and Δ_u, are defined here on the basis of the test results. Because of the non-linearity and the absence of a distinct yield point on the envelope curves, the characteristic values of the loads and displacements were determined using the following two methods.

4.3.1. AISI Standard [1]

According to this method, the peak point (Δ_{max}, P_{max}) is determined as the maximum load and the corresponding displacement on the envelope curves. The elastic point (Δ_e, P_e) is located at $0.4P_{max}$. The ultimate point (Δ_u, P_u) is defined as the point of the 80% post-peak load. The yield point (Δ_y, P_y) is determined using an ideal perfectly elastic–plastic bilinear model that is capable of dissipating an equivalent amount of energy (area $A_1 = A_2$ in Fig. 18a). The initial lateral stiffness k_0 can be determined as the secant stiffness to the load P_e, and point C is the yield point.

4.3.2. ECCS Recommendation [36]

This method for determining the elastic point (Δ_e, P_e), the peak point (Δ_{max}, P_{max}), and the initial stiffness k_0 is the same as that of the AISI Standard. The yield point (Δ_y, P_y) can be obtained as the point of intersection of the elastic line k_0 with the line $0.1k_0$, which is the tangent to the envelope curve of the test specimens, as shown in Fig. 18b. The ultimate point (Δ_u, P_u) is determined as the intersection point of the horizontal yield line with the envelope curve in the downloading branch.

The characteristic values of the loads P_e, P_y, P_{max}, and P_u, as well as the displacements Δ_e, Δ_y,Δ_{max}, and Δ_u, which are determined by the above two methods, are divided by the wall width L (=2400 mm) and the height H (=3000 mm), respectively, to obtain the corresponding loads per unit length P_e', P_y', P_{max}', and P_u' and drift angles θ_e, θ_y, θ_{max}, and θ_u. The characteristic values determined are given in Table 5. The AISI Standard [1] uses the peak load per unit length P_{max}' as the nominal value P_{nom} for the design of CFS-framed shear walls, while the Chinese Standard JGJ 227-2011 [34] uses the yield load per unit length P_y'. The peak load and the yield load per unit length of each test specimen are compared in Fig. 19. From Table 5 and Fig. 19, it can be seen that the difference between the results obtained by the AISI Standard and the ECCS Recommendation is relatively small. Based on the values obtained using the AISI Standard, the following conclusions are drawn:

(1) The shear capacity and lateral stiffness of Specimen F-KB were low. The yield and peak loads were only 1.03 and 1.16 kN/m, respectively, while the failure drift angle was close to 1/25. It is therefore important from an economic perspective to consider the interaction between the type of steel frame and the sheathing method in the design of CFS-framed structures. In Specimen F-XB, the X-shaped bracings substantially increased the load-bearing capacity of the CFS frames. The yield load and peak load of Specimen F-XB were 9.6 and 9.7 times those of Specimen F-KB, respectively.

(2) The strong interaction between the steel frame and SLM layer in the Type B wall specimens significantly increased both the load-bearing capacity and lateral stiffness. The yield loads of the test specimens were 19.27–25.00 kN/m, the peak loads were 21.35–29.10 kN/m, and the shear deformations were relatively small. The drift angles under the peak load were only 1/299–1/106. Because the connections of the knee elements were weak, there was not much improvement in the shear performance of the wall specimens with knee elements. However, local strengthening of the connections of the knee elements using gusset plates increased the yield and peak loads of the CFS walls by approximately 20% and 21%,

Table 5
Characteristic values of loads and displacements.

No.	Specimen	Loading direction	θ_e (rad)	P'_e (kN/m)	θ_{max} (rad)	P'_{max} (kN/m)	AISI Standard				ECCS Recommendation			
							θ_y (rad)	P'_y (kN/m)	θ_u (rad)	P'_u (kN/m)	θ_y (rad)	P'_y (kN/m)	θ_u (rad)	P'_u (kN/m)
1	F-KB	Positive	1/243	0.45	1/42	1.13	1/110	1.00	1/25	0.91	1/114	0.97	1/26	0.97
		Negative	1/305	0.47	1/41	1.18	1/136	1.06	1/25	0.95	1/147	0.98	1/25	0.98
		Average value	1/271	0.46	1/42	1.16	1/121	1.03	1/25	0.93	1/128	0.98	1/26	0.98
2	F-XB	Positive	1/439	4.22	1/107	10.55	1/201	9.19	1/97	8.44	1/189	9.80	1/103	9.80
		Negative	1/399	4.76	1/117	11.90	1/176	10.78	1/104	9.52	1/166	11.41	1/114	11.41
		Average value	1/418	4.49	1/112	11.23	1/188	9.98	1/100	8.98	1/177	10.61	1/108	10.61
3	W-NB-1	Positive	1/1075	9.88	1/125	24.69	1/516	20.58	1/91	19.75	1/578	18.38	1/63	18.38
		Negative	1/1271	10.26	1/106	25.65	1/517	22.69	1/66	20.52	1/737	17.70	1/62	17.70
		Average value	1/1167	10.07	1/115	25.17	1/543	21.64	1/76	20.14	1/648	18.04	1/63	18.04
4	W-NB-2	Positive	1/1339	8.54	1/248	21.35	1/594	19.27	1/107	17.08	1/615	18.63	1/122	18.63
		Negative	1/1622	8.90	1/251	22.23	1/997	19.82	1/102	17.79	1/999	17.10	1/97	17.10
		Average value	1/1463	8.72	1/249	21.79	1/744	19.55	1/105	17.43	1/762	17.86	1/108	17.86
5	W-KB-1	Positive	1/1034	10.10	1/152	25.25	1/472	22.17	1/86	20.20	1/513	20.40	1/87	20.40
		Negative	1/1163	9.54	1/152	23.84	1/525	21.13	1/108	19.08	1/566	19.63	1/109	19.63
		Average value	1/1095	9.82	1/152	24.55	1/498	21.65	1/96	19.64	1/539	20.01	1/97	20.01
6	W-KB-2	Positive	1/1250	8.94	1/120	22.35	1/561	19.95	1/73	17.88	1/636	17.59	1/72	17.59
		Negative	1/1493	9.57	1/116	23.91	1/693	20.65	1/86	19.13	1/833	17.08	1/63	17.08
		Average value	1/1364	9.25	1/118	23.13	1/620	20.30	1/79	18.50	1/721	17.34	1/67	17.34
7	W-KB-S-1	Positive	1/1071	11.53	1/114	28.81	1/498	24.78	1/86	23.05	1/591	20.89	1/82	20.89
		Negative	1/1083	11.64	1/134	29.10	1/506	24.91	1/95	23.28	1/576	21.89	1/89	21.89
		Average value	1/1075	11.58	1/123	28.96	1/502	24.85	1/90	23.17	1/583	21.39	1/85	21.39
8	W-KB-S-2	Positive	1/1339	10.98	1/196	27.43	1/607	24.20	1/127	21.95	1/662	22.15	1/130	22.15
		Negative	1/1224	11.35	1/189	28.37	1/563	24.65	1/143	22.70	1/593	23.38	1/147	23.38
		Average value	1/1277	11.16	1/193	27.90	1/584	24.42	1/136	22.32	1/626	22.76	1/138	22.76
9	W-XB-1	Positive	1/1478	11.54	1/157	28.84	1/612	25.00	1/108	23.07	1/721	21.23	1/102	21.23
		Negative	1/1304	11.51	1/214	28.77	1/611	24.53	1/167	23.02	1/620	24.17	1/175	24.17
		Average value	1/1382	11.52	1/181	28.80	1/612	24.76	1/131	23.05	1/667	22.70	1/129	22.70
10	W-XB-2	Positive	1/1277	10.79	1/203	26.98	1/602	22.85	1/136	21.58	1/613	22.44	1/147	22.44
		Negative	1/1596	10.51	1/299	26.27	1/730	22.94	1/120	21.02	1/730	22.94	1/169	22.94
		Average value	1/1415	10.65	1/242	26.63	1/661	22.90	1/128	21.30	1/667	22.69	1/157	22.69
11	W-NB-CSB	Positive	1/952	8.85	1/172	22.14	1/542	19.23	1/94	17.71	1/564	18.49	1/100	18.49
		Negative	1/1128	8.53	1/162	21.32	1/630	18.75	1/93	17.05	1/713	16.57	1/89	16.57
		Average value	1/1033	8.69	1/167	21.73	1/583	18.99	1/93	17.38	1/630	17.53	1/94	17.53
12	W-XB-CSB	Positive	1/932	10.85	1/129	27.13	1/244	24.58	1/110	21.71	1/233	25.83	1/124	25.83
		Negative	1/1014	11.55	1/167	28.86	1/289	26.30	1/103	23.09	1/281	27.01	1/127	27.01
		Average value	1/971	11.20	1/145	28.00	1/265	25.44	1/106	22.40	1/254	26.42	1/126	26.42

respectively. In addition, the fitting of steel-strap X-shaped bracings not only enhanced the overall stability of the wall frames during construction but also increased their yield and peak loads by 16% and 18%, respectively, compared to those of the wall specimens without bracings. Although the load-bearing capacity of the wall specimens with either joint-strengthened knee elements or X-shaped bracings can be improved to some extent, the constraint of the bracing members decreases the shear drift.

(3) Increasing the vertical load increased the axial compression of the studs, and this decreased the load-bearing capacity and shear deformation of the walls. The peak loads and corresponding displacements of the wall specimens subjected to a vertical load of 60 kN were reduced by 4–13% and 21–58%, respectively, compared to those of the specimens subjected to a vertical load of 30 kN.

(4) The shear capacity of the Type C wall specimens was similar to that of the specimens with SLM sheathing on both sides. However, the usable floor area of a building with Type C walls is increased by the reduced wall thickness achieved by the sheathing method.

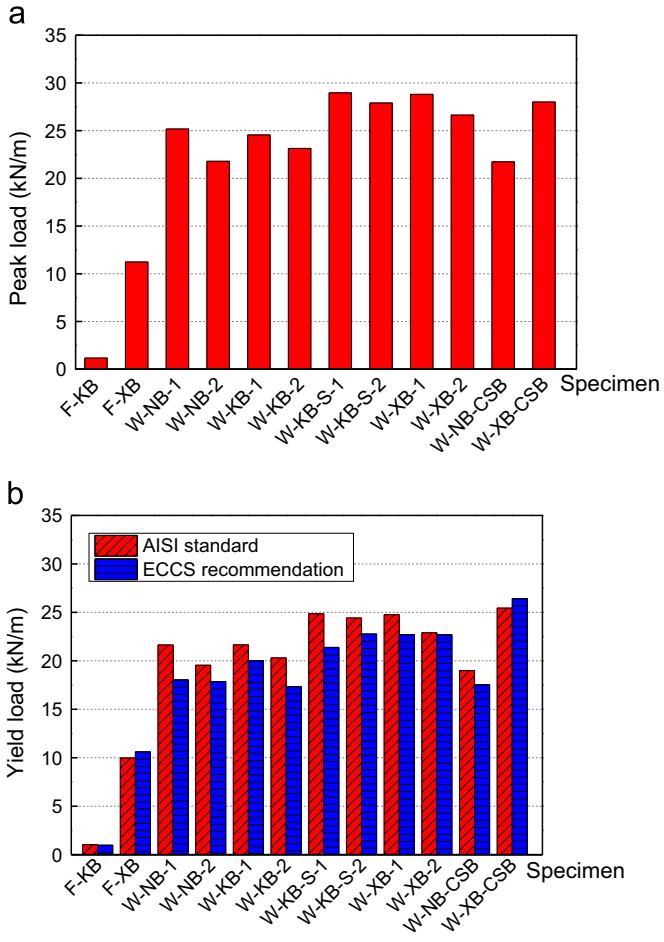

Fig. 19. Characteristic values of loads: (a) peak load and (b) yield load.

4.4. Ductility ratio

The ductility factor (μ) is the ratio of the ultimate displacement Δ_u to the yield displacement Δ_y:

$$\mu = \Delta_u/\Delta_y > 1.0 \tag{5}$$

where the displacements Δ_y and Δ_u are calculated using the methods recommended by AISI [1] and ECCS [36]. The calculated ductility ratios are summarised in Table 6 and illustrated in Fig. 20. The following observations can be made: (1) Specimen F-XB exhibited poor ductility because of the abrupt buckling of the end studs and the resulting rapid decrease in the load. (2) The Type B wall specimens exhibited good ductility because of the interaction between the steel frame and the SLM layer. The installation of the CFS bracing members increased the axial stress of the end studs and decreased the ultimate displacement, resulting in a reduction of the ductility ratio. Local reinforcement of the bottom of the end studs, which appeared to buckle locally under horizontal loads, is recommended in engineering practice to improve the shear capacity and ductility of such walls. (3) The Type C wall specimens exhibited lower ductility than the specimens with SLM sheathing on both sides. This is because the self-drilling screws along the edges of the CSB panels in the former almost failed by bearing or pull-though.

4.5. Lateral stiffness and stiffness degradation

The lateral stiffness of each of the test specimens was determined as the secant stiffness to a load of 0.4 P_{max}, as recommended by ECCS [36]. The results are listed in Table 6. Fig. 21 shows that the weak connections of the knee elements had a negligible effect on the stiffness of the wall specimens. However, the fitting of the joint-strengthened knee-elements and X-shaped bracings increased the stiffness by 9% and 27%, respectively. Because the screw connections of the CSB panels to the CFS frame were weaker than the interaction between the frame and an SLM layer, the Type C wall specimens had lower stiffness than the specimens with SLM sheathing on both sides.

Fig. 22 shows the curves of the secant stiffness versus the drift angle, which reflect the stiffness degradation of each wall specimen during the test, where the locus was determined using the secant stiffness calculated from the peak load points of the first cycle of cycles with the same displacement amplitude. Because the end studs of Specimen F-XB buckled abruptly, its stiffness degradation curve has a catastrophe point, which is undesirable from the perspective of structural seismic behaviour. However, there are no obvious catastrophe points in the stiffness degradation curves of the other wall specimens. The secant stiffness of the walls decreased gradually with increasing displacement, but the stiffness degradation rate was relatively slow.

4.6. Energy absorption

The energy absorption is given by the area under the envelope curve, that is, the load–displacement curve. Table 6 lists the energy absorptions of the different test specimens at the ultimate displacement. Although the results for the ultimate point (Δ_u, P_u) obtained by the methods recommended by AISI [1] and ECCS [36] differ, the differences between the amounts of energy absorbed as calculated by the two methods is relatively small, as shown in Fig. 23. Comparison of the energy absorptions of the different test specimens revealed the following: (1) The energy absorptions of Specimens W-KB-1 and W-XB-1 were 5.5 and 2.4 times those of Specimens F-KB and F-XB, respectively. The energy absorption of CFS-framed shear walls with SLM layers is therefore evidently superior to that of simple steel frames. This is because some energy is dissipated through the bonding slip between the CFS frame and an SLM layer. (2) Because the fitting of X-shaped bracings in CFS walls increases the axial force acting on the end studs, which are prone to local buckling, the energy absorption can be reduced by 24.9–35.9%. (3) The relatively weak strength of the screw connections between the CSB panels and the steel frame caused the energy absorption of the Type C wall specimens to be slightly lower than those of the specimens with SLM sheathing on both sides.

4.7. Strain analysis

The data acquired with the strain gauges were used to evaluate the strain variations during the tests. Positive strain values denote tensile strain, while negative values denote compressive strain. The variations of the strains in the CFS members, including the studs, blocking members, knee elements, and steel-strap X-shaped bracings, are summarised below.

4.7.1. Studs, blocking members, and knee bracing elements

The load–strain (P–ε) curves of the studs, blocking members, and knee elements of Specimen W-KB-S-1 are shown in Fig. 24. Before the peak load, the increases in the strains of the studs of the test specimen were linear. At the peak load, the strain of the end studs was close to the yield strain, but those of the three interior studs were still small. Meanwhile, the strains of the blocking members and knee elements were within the elastic range. Due to the weak connections of the CFS members, the steel frame mainly resisted the horizontal load by means of the resultant overturning

Table 6
Test parameters of test specimens.

No.	Specimen	Loading direction	Δ_e (mm)	P_e (kN)	k_0 (kN/mm)	μ_{AISI}	μ_{ECCS}	E_{AISI} (J)	E_{ECCS} (J)
1	F-KB	Positive	12.35	1.09	0.09	4.35	4.35	254	244
		Negative	9.84	1.13	0.12	5.46	5.80	280	273
		Average value	11.09	1.11	0.10	4.85	4.98	267	259
2	F-XB	Positive	6.84	10.13	1.48	2.07	1.83	515	486
		Negative	7.52	11.42	1.52	1.70	1.46	528	465
		Average value	7.18	10.78	1.50	1.87	1.63	522	476
3	W-NB-1	Positive	2.79	23.70	8.50	5.65	9.15	1447	2152
		Negative	2.36	24.62	10.43	8.75	11.86	2344	2465
		Average value	2.57	24.16	9.47	7.11	10.35	1896	2309
4	W-NB-2	Positive	2.24	20.49	9.16	5.54	5.03	1678	1530
		Negative	1.85	21.35	11.54	9.78	11.92	1427	1497
		Average value	2.05	20.92	10.23	7.12	7.43	1553	1514
5	W-KB-1	Positive	2.90	24.24	8.37	5.50	5.90	1693	1669
		Negative	2.58	22.89	8.89	4.87	5.17	1264	1247
		Average value	2.74	23.56	8.63	5.20	5.55	1479	1458
6	W-KB-2	Positive	2.40	21.45	8.95	7.63	8.84	1827	1864
		Negative	2.01	22.96	11.44	8.09	13.27	1630	2179
		Average value	2.20	22.21	10.20	7.84	10.76	1729	2022
7	W-KB-S-1	Positive	2.80	27.66	9.87	5.76	7.19	1884	1980
		Negative	2.77	27.94	10.08	5.35	6.48	1719	1830
		Average value	2.79	27.80	9.98	5.55	6.83	1802	1905
8	W-KB-S-2	Positive	2.24	26.34	11.75	4.70	5.09	1205	1195
		Negative	2.45	27.23	11.10	3.95	4.04	1086	1051
		Average value	2.35	26.79	11.42	4.31	4.54	1146	1123
9	W-XB-1	Positive	2.03	27.69	13.65	5.68	7.05	1521	1602
		Negative	2.30	27.62	11.99	3.65	3.54	911	867
		Average value	2.17	27.65	12.82	4.66	5.16	1216	1235
10	W-XB-2	Positive	2.35	25.90	11.02	4.43	4.17	1073	984
		Negative	1.88	25.22	13.40	6.08	4.33	1261	879
		Average value	2.12	25.56	12.21	5.18	4.24	1167	932
11	W-NB-CSB	Positive	3.15	21.25	6.75	5.78	5.63	1351	1258
		Negative	2.66	20.46	7.69	6.76	7.98	1340	1397
		Average value	2.91	20.86	7.22	6.23	6.67	1346	1328
12	W-XB-CSB	Positive	3.22	26.05	8.09	2.22	1.88	1248	1076
		Negative	2.96	27.71	9.36	2.81	2.20	1515	1172
		Average value	3.09	26.88	8.73	2.49	2.03	1382	1124

moment produced by the axial tensile or compressive forces exerted by the end studs.

4.7.2. Steel-strap x-shaped bracings

The load–strain (P–ε) curves of the test specimens with steel-strap X-bracings are shown in Fig. 25. During the testing of Specimen F-XB, the tensile strap was always tight, while the compressive strap was slack. In Fig. 25a, the measurements obtained with the strain gauges on opposite sides of the same point on the slack strap are of opposite signs, which indicate the buckling of the compressive strap. Under the peak load, the strain of the tensile strap was at the yield stage, as shown in Fig. 25b. Because the strong interaction between the steel frame and the SLM layers weakened the contribution of the X-shaped bracings to the lateral performance, the strain of the X-shaped bracings in Specimen W-XB-1 were low compared to that of the bracings in Specimen F-XB. In addition, the restriction of the out-of-plane deformation of the compressive strap by the outside SLM layer caused the strain measurements on opposite sides of the same point on the compressive strap to be negative (Fig. 25c). This restriction limits the buckling of the compressive strap and improves the applicability of CFS walls.

5. Comparison with CFS walls with traditional sheathing

The shear behaviour of the CFS-framed shear walls with SLM sheathing is compared with that of CFS-framed shear walls with traditional sheathing in Table 7. It can be seen that the peak loads of the walls with SLM sheathing on both sides were 64.6%, 49.8%,

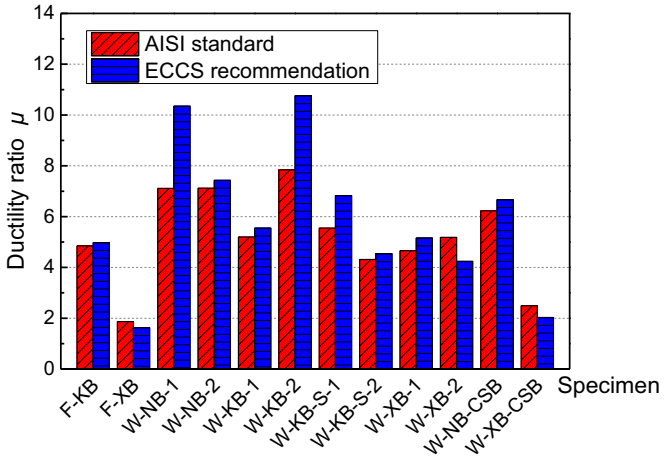

Fig. 20. Ductility ratios of test specimens.

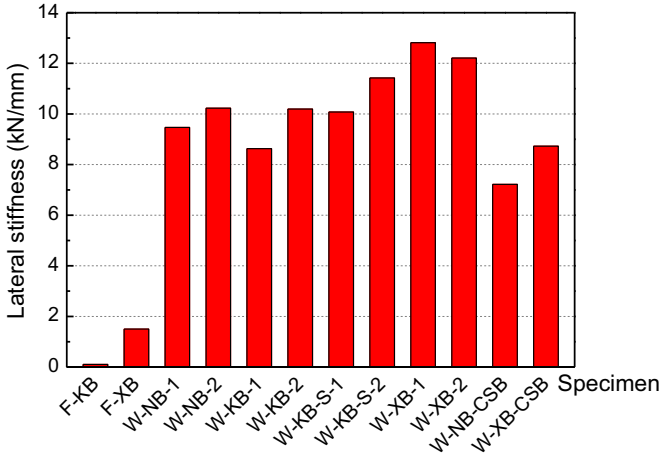

Fig. 21. Lateral stiffness of test specimens.

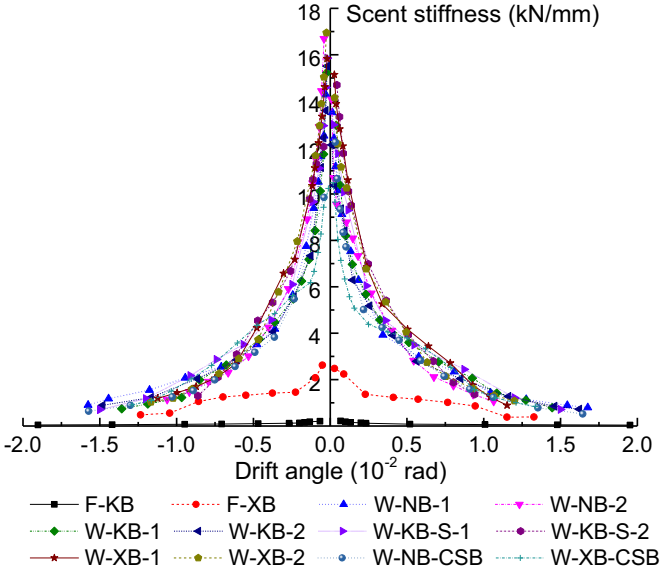

Fig. 22. Stiffness degradation curves of test specimens.

and 20.0% higher than those of walls sheathed with gypsum boards, CSB panels, and OSB panels, respectively. The interaction between the CFS frame and the SLM layers is evidently stronger than the connections between the CSB panels and the steel frame.

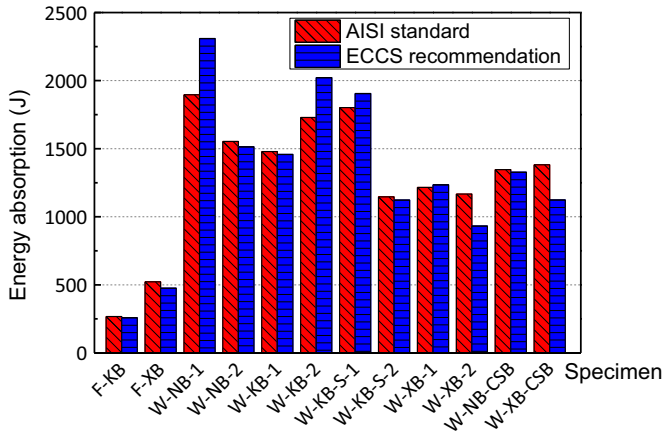

Fig. 23. Energy absorptions of test specimens.

The lateral stiffness of CFS walls with SLM sheathing on both sides is more than eight times greater than that of walls with traditional panels, and the shear deformations of walls with SLM sheathing on both sides are only 18–28% of those of walls with gypsum boards, CSB panels, or OSB panels. Moreover, the new sheathing technique using SLM modestly improves the ductility of a CFS shear wall.

6. Conclusions and recommendations

A total of twelve full-scale specimens, including two bare CFS frames, eight CFS-framed shear walls with SLM sheathing on both sides, and two CFS-framed shear walls with an SLM layer on the front side and CSB panels on the back side were tested under reversed cyclic loading. Based on the test results, the following conclusions are drawn:

(1) The failure modes of a CFS frame with knee elements are tilting or pull-out of the screws used to connect the knee elements to the blocking members and local buckling of the flange of the blocking members at the connection to the knee elements. Both the load-bearing capacity and lateral stiffness of this type of steel frame are low. When a CFS frame with steel-strap X-shaped bracings is subjected to cyclic loading, there is alternating tightening of the tensile strap and slackening of the compressive strap. Failure eventually occurs due to flexural–torsional buckling of the end studs after local buckling of the web. In addition, under the peak load, the stress of the tensile strap reaches the yield level.

(2) A CFS-framed shear wall with SLM sheathing on both sides fails by local buckling of the bottom of the end studs and relative slippage between the steel frame and the outside SLM layer. Although cracking of the mortar layer occurs, the overall stability and integrity of the wall are well preserved at the ultimate stage. In a CFS-framed shear wall with an SLM layer on the front side and CSB panels on the back side, in addition to the above failure modes, there is also apparent relative movement of the individual CSB panels and separation of the panels from the steel frame. This is due to pull-through of the self-drilling screws along the edges of the panels.

(3) Because of the strong interaction between the steel frame and the SLM layers, the load-bearing capacity and lateral stiffness of a CFS-framed shear wall with SLM sheathing on both sides are quite high. Because of a certain amount of slippage between the steel frame and the outside SLM layer at the ultimate stage, CFS walls with SLM sheathing exhibit good

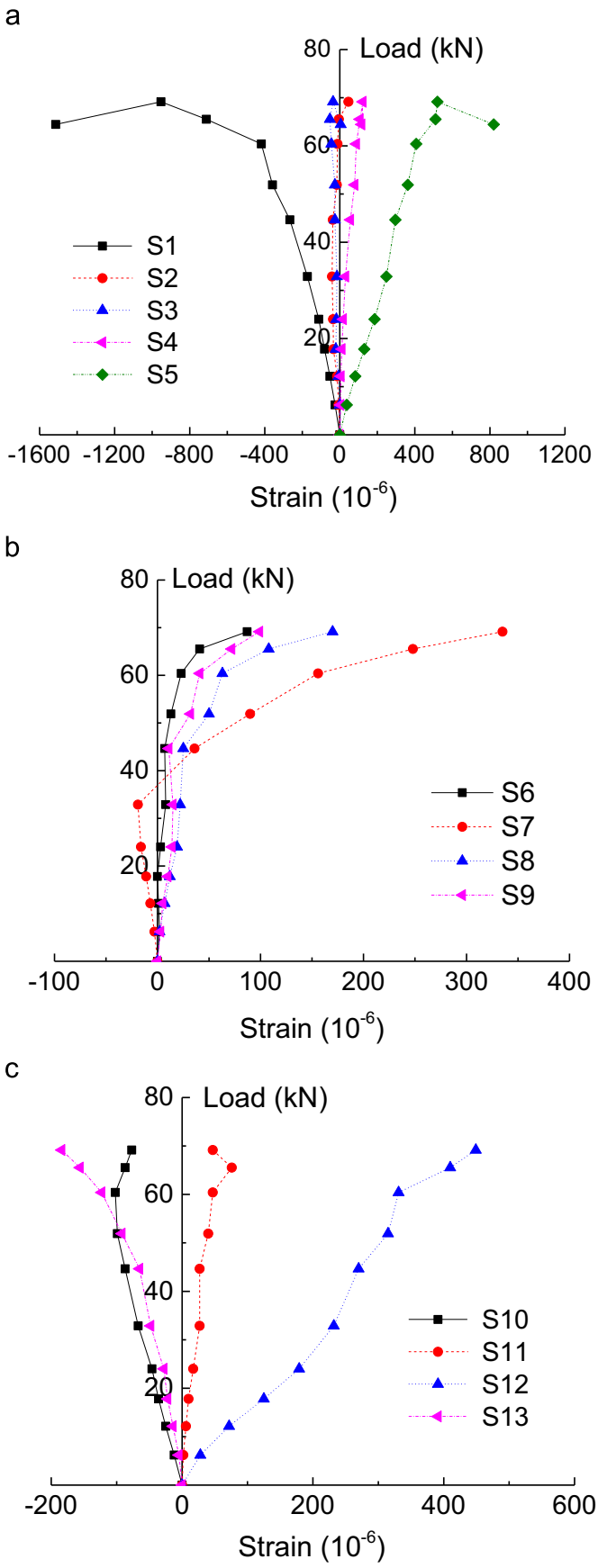

Fig. 24. Load–strain curves of Specimen W-KB-S-1: (a) studs, (b) blockings, (c) knee elements.

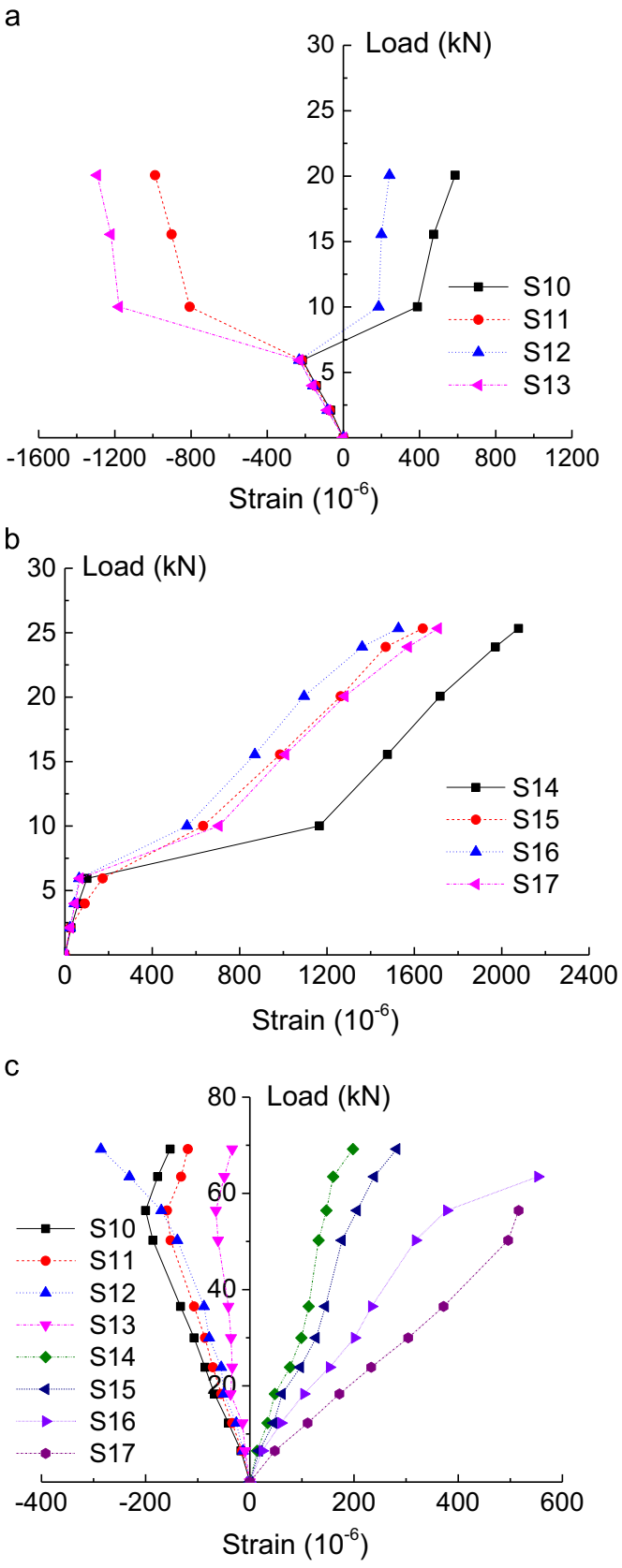

Fig. 25. Load–strain curves of steel-strap X-shaped bracings: (a) compressive strap in Specimen F-XB, (b) tensile strap in Specimen F-XB, and (c) steel strap in Specimen W-XB-1.

Table 7
Comparison of present test results with those in Ref. [6].

Study	Specimen label	Aspect (mm × mm)	Type of sheathing	Studs-tracks	P_{max} (kN/m)	θ_{max} (rad)	k_0[a] (kN/mm)	μ_{AISI}
Present	W-NB-1	2400 × 3000	30-mm SLM layer on both sides	C89 × 35 × 10.6 × 1.0, U92.2 × 41.5 × 1.2	25.17	1/115	11.83	7.11
Ref. [6]	FFM-G12-FT	2400 × 2400	12-mm gypsum boards on both sides	C92 × 65 × 12 × 1.6, U95.2 × 45 × 1.6	15.29	1/32	1.41	6.68
	FFM-C09-HT	1200 × 2400	9-mm CSB panels on both sides	C92 × 65 × 12 × 1.6, U95.2 × 45 × 1.6	16.80	1/21	0.92	3.52
	FFM-O12-FO	2400 × 2400	12-mm OSB panels on one side	C92 × 65 × 12 × 1.6, U95.2 × 45 × 1.6	20.98	1/31	1.43	3.12

[a] Stiffness was calculated using $k_0 = \alpha[P/\Delta]_{0.4P_{max}}$, where α is the aspect ratio of the wall specimens [6].

ductility and energy absorption, and this restricts the propagation of cracks in the mortar layer.

(4) Because of their weak connection, knee elements do not significantly improvement the shear capacity and lateral stiffness of a CFS wall. The use of joint-strengthened knee elements and X-shaped bracings increases the load-bearing capacity but decreases the drift angle of a wall with SLM sheathing on both sides.

(5) Increasing the vertical load reduces the load-bearing capacity and shear deformation of a wall with SLM sheathing but has little effect on the lateral stiffness. Because increasing the vertical load strengthens the bonding slippage between the steel frame and the outside SLM layer, the 'pinching' effect observed in the hysteresis curve of a CFS-framed shear wall should therefore be moderated.

(6) The self-drilling screws used to connect the CSB panels to the steel frames are weaker than the interaction between the CFS frame and the SLM layer. This causes the shear capacity of the wall with SLM sheathing on the front side and CSB panels on the back side to be slightly lower than that of a CFS-framed shear wall with SLM sheathing on both sides. Moreover, the former type of wall is thinner and thus increases the usable floor area of a building in which it is used.

(7) The peak loads of a CFS wall with SLM sheathing on both sides are 64.6%, 49.8%, and 20.0% higher than those of similar walls sheathed with gypsum boards, CSB panels, and OSB panels, respectively. Compared to the use of traditional sheathing, the proposed use of SLM sheathing not only considerably increases the lateral stiffness of a CFS wall but also modestly improves the ductility of the overall structure.

The present work was a preliminary experimental study on the shear capacity of CFS-framed shear walls with SLM sheathing. Based on the test results, the following recommendations are made to facilitate further study of the proposed type of CFS-framed shear walls.

(1) Because the bottom parts of the end studs are prone to local buckling during testing, they should be strengthened to improve the shear capacity, ductility, and energy absorption of the wall.

(2) Relative slip between the steel frame and the SLM layers was observed in the present tests, and it is therefore necessary to experimentally investigate the behaviour of the bonding slip to determine the values of relevant parameters for numerical and theoretical analyses of the proposed type of wall.

(3) Considering the desire for enhanced shear capacity, the amount of lightweight mortar that is sprayed on both sides of the steel frame should be reasonably reduced. This would also reduce the cost of the wall and increase the usable floor area of the building.

Acknowledgement

The authors would like to acknowledge the support provided by the Science and Technology Fund Project (2012-K2-17) of the Ministry of Housing and Urban–Rural Development of P.R. China and the Major Science and Technology Innovation Fund Project of Shaanxi Province of P.R. China (2009ZDKG-66) . The materials for the construction of the test specimens were generously provided by Guangzhou CRUPE System Building Materials Co., Ltd. Special thanks are expressed to Ying-Chun Wang, Qiu-Li Zhao, Carrie Yuen, Ke-Long Li, Yi-Jun Wang, Da-Yu Shao, Lin-Wei Zhao, Rui Bai, and Yue-Chen Li for their contributions throughout the project.

Appendix A. Supplementary material

Supplementary data associated with this article can be found in the online version at http://dx.doi.org/10.1016/j.tws.2015.09.024.

References

[1] American Iron and Steel Institute (AISI), North American Standard for Cold-formed Steel Framing—Lateral Design, AISI S213, Washington, DC, USA, 2007.
[2] R.L. Serrette, H. Nguyen, G. Hall, Shear Wall Values for Light Weight Steel Framing, Report No. LGSRG-3-96, Department of Civil Engineering, Santa Clara University Santa Clara, CA, USA, 1996.
[3] R.L. Serrette, Additional Shear Wall Values for Light Weight Steel Framing, Report No. LGSRG-1-97, Department of Civil Engineering, Santa Clara University Santa Clara, CA, USA, 1997.
[4] R.L. Serrette, Performance of Cold-Formed Steel-framed Shear Walls: Alternative Configurations, Report No. LGSRG-06-02, Department of Civil Engineering, Santa Clara University Santa Clara, CA, USA, 2002.
[5] L.A. Fülöp, D. Dubina, Performance of wall-stud cold-formed shear panels under monotonic and cyclic loading: Part I: experimental research, Thin-Walled Struct. 42 (2) (2004) 321–338.
[6] C.L. Pan, M.Y. Shan, Monotonic shear tests of cold-formed steel wall frames with sheathing, Thin-Walled Struct. 49 (2) (2011) 363–370.
[7] M. Nithyadharan, V. Kalyanaraman, Behavior of cold-formed steel shear wall panels under monotonic and reversed cyclic loading, Thin-Walled Struct. 60 (11) (2012) 12–23.
[8] P. Liu, K.D. Peterman, B.W. Schafer, Impact of construction details on OSB-sheathed cold-formed steel framed shear walls, J. Constr. Steel Res. 101 (2014) 114–123.
[9] M. Zeynalian, H.R. Ronagh, Seismic performance of cold formed steel walls sheathed by fibre-cement board panels, J. Constr. Steel Res. 107 (2015) 1–11.
[10] U.S. Army Corps of Engineers, Engineering and Construction Division, Directorate of Military Program, Technical Instructions: Design of Cold-formed Load Bearing Steel Systems and Masonry Veneer/steel Stud Walls, TI 809-07, Washington, DC, USA, 2006.
[11] M. Zeynalian, H.R. Ronagh, A numerical study on seismic characteristics of knee-braced cold formed steel shear walls, Thin-Walled Struct. 49 (12) (2011) 1517–1525.
[12] M. Zeynalian, H.R. Ronagh, S. Hatami, Seismic characteristics of K-braced cold-formed steel shear walls, J. Constr. Steel Res. 77 (10) (2012) 23–31.
[13] M. Zeynalian, H.R. Ronagh, An experimental investigation on the lateral behavior of knee-braced cold-formed steel shear walls, Thin-Walled Struct. 51 (2) (2012) 64–75.
[14] H. Moghimi, H.R. Ronagh, Performance of light-gauge cold-formed steel strap-braced stud walls subjected to cyclic loading, Eng. Struct. 31 (1) (2009) 69–83.

[15] H. Moghimi, H.R. Ronagh, Better connection details for strap-braced CFS stud walls in seismic regions, Thin-Walled Struct. 47 (2009) 122–135.
[16] O. Iuorio, V. Macillo, M.T. Terracciano, T. Pali, L. Fiorino, R. Landolfo, Seismic response of Cfs strap-braced stud walls: experimental investigation, Thin-Walled Struct. 85 (2014) 466–480.
[17] V. Macillo, O. Iuorio, M.T. Terracciano, L. Fiorino, R. Landolfo, Seismic response of CFS strap-braced stud walls: theoretical study, Thin-Walled Struct. 85 (2014) 301–312.
[18] R. Serrette, I. Lam, H. Qi, H. Hernandez, A. Toback, Cold-formed steel frame shear walls utilizing structural adhesives, J. Struct. Eng. ASCE 132 (4) (2006) 591–599.
[19] R. Serrette, D.P. Nolan, Reversed cyclic performance of shear walls with wood panels attached to cold-formed steel with pins, J. Struct. Eng. ASCE 135 (8) (2009) 959–967.
[20] C. Yu, Shear resistance of cold-formed steel framed shear walls with 0.686 mm, 0.762 mm, and 0.838 mm steel sheet sheathing, Eng. Struct. 32 (6) (2010) 1522–1529.
[21] C. Yu, Y. Chen, Detailing recommendations for 1.83 m wide cold-formed steel shear walls with steel sheathing, J. Constr. Steel Res. 67 (1) (2011) 93–101.
[22] J. DaBreo, N. Balh, C. Ong-Tone, C.A. Rogers, Steel sheathed cold-formed steel framed shear walls subjected to lateral and gravity loading, Thin-Walled Struct. 74 (2014) 232–245.
[23] A. Shakibanasab, N.K.A. Attari, M. Salari, A statistical and experimental investigation into the accuracy of capacity reduction factor for cold-formed steel shear walls with steel sheathing, Thin-Walled Struct. 77 (4) (2014) 56–66.
[24] S. Mohebbi, R. Mirghaderi, F. Farahbod, A.B. Sabbagh, Experimental work on single and double-sided steel sheathed cold-formed steel shear walls for seismic actions, Thin-Walled Struct. 91 (2015) 50–62.
[25] L.G. Vigh, A.B. Liel, G.G. Deierlein, E. Miranda, S. Tipping, Component model calibration for cyclic behavior of a corrugated shear wall, Thin-Walled Struct. 75 (2) (2014) 53–62.
[26] W. Mowrtage, N. Hasan, B. Pekmezci, H.N. Atahan, Loading carrying capacity enhancement of cold-formed steel walls using shotcreted steel sheets, Thin-Walled Struct. 60 (11) (2012) 145–153.
[27] Ministry of Housing and Urban–Rural Development of P.R. China, General Administration of Quality Supervision, Inspection, and Quarantine of P.R. China, Technical Code for Cold-formed Thin-wall Steel Structures, GB 50018-2002. Beijing, PRC, 2002.
[28] General Administration of Quality Supervision, Inspection and Quarantine of P.R. China, Drilling Screws With Tapping Screw Thread, GB 15856-2002, Beijing, PRC, 2002.
[29] K. Velchev, G. Comeau, N. Balh, C.A. Rogers, Evaluation of the AISI S213 seismic design procedures through testing of strap braced cold-formed steel walls, Thin-Walled Struct. 48 (10–11) (2010) 846–856.
[30] General Administration of Quality Supervision, Inspection and Quarantine of P.R. China, Standardization Administration of P.R. China, Metallic Materials—Tensile Testing—Part 1: Method of Test at Room Temperature, GB/T 228.1-2010, Beijing, PRC, 2011.
[31] Ministry of Housing and Urban–Rural Development of P.R. China, Standard for Test Method of Performance on Building Mortar, JGJ/T 70-2009, Beijing, PRC, 2009.
[32] General Administration of Quality Supervision, Inspection and Quarantine of P.R. China, Test Methods of Evaluating the Properties of Wood-Based Panels and Surface Decorated Wood-Based Panels, GB/T 17657-1999, Beijing, PRC, 1999.
[33] American Society for Testing and Materials (ASTM), Standard Test Methods for Cyclic (Reversed) Load Test for Shear Resistance of Walls for Buildings, ASTM E2126-07, West Conshohocken, USA, 2007.
[34] Ministry of Housing and Urban–Rural Development of P.R. China, Technical Specification for Low-rise Cold-Formed Thin-walled Steel Buildings, JGJ 227-2011, Beijing, PRC, 2011.
[35] B. Liu, J.P. Hao, W.H. Zhong, Y.C. Wang, Z.G. Huang, Q.L. Zhao, Experimental research on seismic behavior of cold-formed thin-wall steel framing walls with sprayed thermal insulation material, J. Build. Struct. 35 (1) (2014) 85–92 (in Chinese).
[36] European Convention for Construction Steelwork, Recommended Testing Procedure for Assessing the Behaviour of Structural Elements Under Cyclic Loads, 1985.